

# GS-ROR: 3D Gaussian Splatting for Reflective Object Relighting via SDF Priors

ZUO-LIANG ZHU, Nankai University, China

BEIBEI WANG<sup>†</sup>, Nanjing University, China

JIAN YANG<sup>†</sup>, Nankai University, China

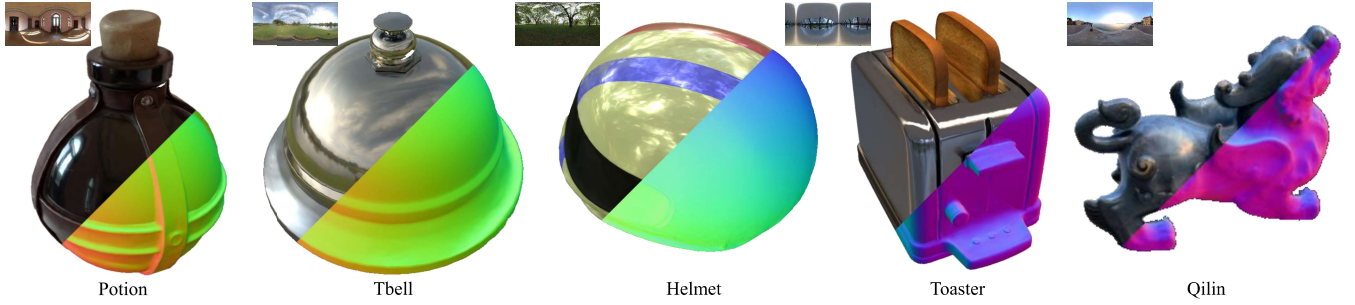


Fig. 1. We present an SDF-aided Gaussian Splatting framework for Reflective Object Relighting (GS-ROR) from multi-view images. We show five relighting results with reflective highlights (left) and their normal estimation (right), including POTION and TBELL from NeRO [Liu et al. 2023], HELMET and TOASTER from Ref-NeRF [Verbin et al. 2022], and QILIN from NeLLF++ [Zhang et al. 2023], where QILIN is from the real scene. Our method demonstrates a robust geometry reconstruction for reflective surfaces and faithful material decomposition, leading to photo-realistic and real-time reflective object relighting.

3D Gaussian Splatting (3DGS) has shown a powerful capability for novel view synthesis due to its detailed expressive ability and highly efficient rendering speed. Unfortunately, creating relightable 3D assets with 3DGS is still problematic, particularly for reflective objects, as its discontinuous representation raises difficulties in constraining geometries. Inspired by previous works, the signed distance field (SDF) can serve as an effective way for geometry regularization. However, a direct incorporation between Gaussians and SDF significantly slows training. To this end, we propose GS-ROR for reflective objects relighting with 3DGS aided by SDF priors. At the core of our method is the *mutual supervision* of the depth and normal between deferred Gaussians and SDF, which avoids the expensive volume rendering of SDF. Thanks to this mutual supervision, the learned deferred Gaussians are well-constrained with a minimal time cost. As the Gaussians are rendered in a deferred shading mode, while the alpha-blended Gaussians are smooth, individual Gaussians may still be outliers, yielding floater artifacts. Therefore, we further introduce an SDF-aware pruning strategy to remove Gaussian outliers, which are located distant from the surface defined by SDF, avoiding the floater issue. Consequently, our method outperforms the existing Gaussian-based inverse rendering methods in terms of relighting quality. Our method also exhibits competitive relighting quality compared to NeRF-based methods with at most 25% of training time and allows rendering at 200+ frames per second on an RTX4090.

CCS Concepts: • **Computing methodologies** → **Rendering**.

Additional Key Words and Phrases: neural rendering, Gaussian splatting, relighting

<sup>†</sup>Corresponding author.

Authors' addresses: Zuo-Liang Zhu, Nankai University, China, nkuzhuzl@gmail.com; Beibei Wang<sup>†</sup>, Nanjing University, China, beibei.wang@nju.edu.cn; Jian Yang<sup>†</sup>, Nankai University, China, csjyang@nankai.edu.cn.

## 1 INTRODUCTION

Creating relightable 3D assets from multi-view images has been a long-standing and challenging task in computer graphics and vision, as the decomposition of lighting, materials, and geometries is highly ill-posed. Particularly, the decomposition becomes more difficult for reflective objects, as their appearances are highly view-dependent, and a minor error on the surface leads to a significant difference. Existing approaches [Li et al. 2024; Liu et al. 2023] have shown impressive relighting quality for reflective objects by leveraging the neural radiance field (NeRF) and the signed distance field (SDF). Unfortunately, these methods require a long training and rendering time. In this paper, we aim at reflective objects relighting given multi-view images, simultaneously achieving high-quality relighting and short training/rendering time costs.

Most recently, Kerbl et al. [2023] proposed 3D Gaussian Splatting (3DGS), boosting the rendering speed significantly and achieving more detailed appearance modeling. A concurrent work [Ye et al. 2024] has introduced deferred Gaussian splatting for reflective objects, significantly improving the novel view synthesis (NVS) quality. Despite the impressive NVS quality, the relighting with 3DGS becomes problematic due to the Gaussians' discontinuity and high flexibility, especially for reflective objects. Extensive efforts have been made to improve the relighting quality by regularizing the geometry in terms of the normal and depth [Gao et al. 2024; Jiang et al. 2024; Liang et al. 2024]. However, they still suffer from erroneous surfaces and floater artifacts for reflective objects.

In this paper, we propose a novel framework GS-ROR for reflective objects relighting by leveraging SDF priors in the deferred Gaussian splatting. A direct incorporation between Gaussians and SDF significantly slows training, due to the expensive computational cost

of SDF rendering. For this, we propose to supervise the deferred Gaussians and SDF mutually in our framework, so-called *mutual-supervision*, which allows constraining deferred Gaussians with SDFs while avoiding SDF rendering. Specifically, the depth/normal of deferred Gaussians is supervised by SDF for regularization, while the SDF is supervised by Gaussians via the depth/normal rather than SDF rendering. This way, the learned deferred Gaussians are better constrained with a minimal computational cost. However, we still notice that Gaussians have floater artifacts occasionally, as the deferred Gaussians (with alpha blending) rather than individual Gaussians are constrained by SDF. Therefore, we introduce an SDF-aware pruning strategy to remove Gaussian outliers to avoid this floater issue. Consequently, our method outperforms the existing Gaussian-based inverse rendering methods in terms of relighting quality. Meanwhile, it exhibits competitive relighting quality compared to NeRF-based methods with at most 25% of training time. It also allows real-time rendering of reflective objects with 200+ frames per second on an RTX4090. To summarize, our main contributions include

- a GS-ROR framework for reflective object relighting, achieving high-quality relighting while maintaining short training time and allowing real-time rendering,
- a mutual supervision approach between deferred Gaussians and the SDF, producing robust geometry and avoiding local minima with minimal computational increase, and
- an SDF-aware Gaussian pruning strategy, which prunes outlier Gaussian, avoiding the float artifacts.

## 2 RELATED WORK

### 2.1 Neural representations for multi-view stereo

Since the presence of NeRF [Mildenhall et al. 2020], numerous neural implicit representations [Barron et al. 2022; Chen et al. 2022; Fridovich-Keil et al. 2022; Müller et al. 2022] have been proposed and gained remarkable progress in the field of multi-view stereo. These NeRF-based models adopt Multi-Layer Perceptrons (MLPs) [Barron et al. 2021, 2022; Verbin et al. 2022] or grid-like representations [Chen et al. 2022; Fridovich-Keil et al. 2022; Müller et al. 2022] to represent geometry and view-dependent appearance, optimized via volume rendering. Subsequently, NeuS [Wang et al. 2021] links the SDF with the density in NeRF and enables the optimization of surfaces with volume rendering. With extra regularization, these SDF-based models [Li et al. 2023; Rosu and Behnke 2023; Wang et al. 2023] achieve detailed surface reconstruction from RGB images. Owing to carefully designed architectures and specific optimization, some methods [Fridovich-Keil et al. 2022; Müller et al. 2022] enable fast training and real-time radiance field rendering.

3DGS [2023] sheds light on the multi-view stereo in the rasterization framework, providing impressive real-time NVS results. 3DGS utilizes the discrete explicit 3D Gaussian primitive and projects these primitives onto the image plane to obtain the pixel color via alpha blending, which avoids the consuming sampling operation. However, 3DGS imposes no geometry constraint while optimizing, leading to noisy depth and normal, which hinders the usage of 3DGS in many downstream tasks. To resolve this issue, existing methods construct different constraints on Gaussians by introducing

2D Gaussians [Huang et al. 2024] or Gaussian Surfels [Dai et al. 2024]. SuGaR [Guédon and Lepetit 2024] extracts a mesh from the Gaussians and binds the flattened Gaussians to the surface to optimize further. These methods improve the geometry quality significantly, which is orthogonal to our relighting framework and can further improve our relighting quality. We leave it for future work.

Several previous works introduce SDF into 3DGS. NeuSG [Chen et al. 2023] introduces SDF into 3DGS to improve the details of surface reconstruction by optimizing NeuS and 3DGS jointly. Despite the high quality of the reconstructed surface, the training time is tens of times longer than 3DGS. GSDF [Yu et al. 2024] utilizes the depth from Gaussian to guide sampling for SDF, but they still need to render color in the SDF branch, leading to higher efficiency. While our method also incorporates the SDF and Gaussians, the key difference is that it drops SDF rendering, improving the geometry quality with a low time cost.

### 2.2 Inverse rendering

Inverse rendering aims to decompose geometry, material, and light from multi-view RGB images. Most existing methods adopt the geometry formulation from NeRF in either density or SDF manner, namely NeRF-based method. In terms of material modeling, most methods utilize the Disney Principled BRDF model [McAuley et al. 2013], while NeRFactor [Zhang et al. 2021b] pretrains a BRDF MLP with a measured BRDF dataset. Considering the light modeling, early works [Bi et al. 2020; Boss et al. 2021a,b; Zhang et al. 2022a, 2021a] consider direct light only, and more recent works [Jin et al. 2023; Srinivasan et al. 2021; Yang et al. 2023; Zhang et al. 2023, 2022b] model indirect lighting and visibility, leading to a higher-quality decomposition. NeRF Emitter [Ling et al. 2024] incorporates NeRF as a non-distant environment emitter and uses importance sampling of NeRF to reduce rendering variance. However, these NeRF-based methods suffer from slow rendering speed and high memory usage in training.

More recently, Gaussian-based inverse rendering methods have begun to emerge. These methods regularize Gaussians to obtain better geometry in various ways. Gaussian Shader [Jiang et al. 2024] and GIR [Shi et al. 2023] link the shortest axis of Gaussian with the normal. The Gaussian shader, Relightable Gaussian [Gao et al. 2024], and GS-IR [Liang et al. 2024] supervise the Gaussian normal with the depth normal. To model the indirect illumination, Relightable Gaussian, GIR, and GS-IR compute the visibility via one-step ray tracing and represent the indirect illumination with SH coefficients. All these Gaussian-based relighting methods cannot relight reflective objects, while our method enables such scenarios.

### 2.3 Reflective objects NVS and relighting

As a special and challenging case, NVS and relighting of reflective objects have drawn much attention. Ref-NeRF [Verbin et al. 2022] replaces the outgoing radiance with the incoming radiance and models the shading explicitly with an integrated direction encoding (IDE) to improve the quality of reflective materials. MS-NeRF [Yin et al. 2023] designs a multi-space neural representation to model the reflection of mirror-like planes. Spec-NeRF [Ma et al. 2024] introduces a learnable Gaussian directional encoding to better model view-dependent

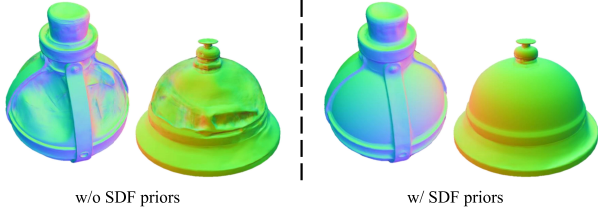


Fig. 2. The geometry from Gaussian is under-constrained and thus erroneous, while it is much better after utilizing the priors from the SDF.

effects. Spec-Gaussian [Yang et al. 2024] uses anisotropic spherical Gaussian to model view-dependent highlights. 3DGS-DR [Ye et al. 2024], as a concurrent work, introduces deferred shading into 3DGS. We also utilize a deferred framework, but for relighting, and together with other key components.

Another group of methods enables relighting for reflective materials. NeRO [Liu et al. 2023] proposes a novel light representation consisting of two MLPs for direct and indirect light, respectively. With explicit incorporation of the rendering equation, NeRO reconstructs reflective objects of high quality. Wang et al. [2024] represent the indirect light with a 5-dimensional function, so-called the 5D neural plenoptic function. Thanks to material-aware integral positional encoding, their method reduces the light sample per pixel during training and provides more accurate material decomposition. TensoSDF [Li et al. 2024] designs a roughness-aware incorporation between the radiance and reflectance field for robust geometry reconstruction and proposes a novel tensorial representation with SDF, enabling fast SDF query. Although their representation is faster than the original SDF, it still needs hours of training time and cannot achieve real-time rendering. DeferredGS [Wu et al. 2024] utilizes the idea of deferred shading to improve the quality of the reflective object relighting in the Gaussian framework. However, their method needs to distill a reasonable geometry from a pretrained SDF, taking more than 3 hours and thus losing the efficiency in training. Our method takes a further step in the reflective object relighting with 3D Gaussians and provides high-quality relighting results while keeping highly efficient training and rendering.

### 3 PRELIMINARIES AND MOTIVATION

In this section, we briefly review two ways for 3D scene representations and then discuss our motivation.

**3D Gaussian Splatting.** 3DGS represents a scene with a set of 3D Gaussians whose distribution is defined as

$$G(x) = e^{-\frac{1}{2}(x-\mu)^T \Sigma^{-1}(x-\mu)}, \quad (1)$$

where  $x$  is a position in the scene,  $\mu$  is the mean of the Gaussian, and  $\Sigma$  denotes the covariance matrix of the 3D Gaussian, which is factorized into a scaling matrix  $S$  and a rotation matrix  $R$  as  $\Sigma = RSS^T R^T$ . To render an image, 3DGS projects the 3D Gaussians onto the image plane and employs alpha blending on the sorted 2D Gaussians as

$$C = \sum_{i=0}^n c_i \alpha_i \prod_{j=1}^{i-1} (1 - \alpha_j), \quad (2)$$

where  $c_i$  is the color of each Gaussian, and  $\alpha_i$  is given by evaluating a projected 2D Gaussian with covariance  $\Sigma'$  multiplied with a learned per-point opacity.

**TensoSDF.** An SDF expresses a scene by encoding the distance from the surface of an object, which can be expressed implicitly by an MLP [Wang et al. 2021] or in a hybrid way by combining explicit grids with a tiny MLP [Li et al. 2024], which allows more efficient training and rendering. Depth and normal are two significant attributes of geometry. In SDF, The point-wise depth  $D_i$  is defined as the distance from the camera to the sample, and the point-wise normal  $\mathbf{n}_i$  is the gradient of SDF  $\nabla_x$  w.r.t. position  $x$  [Zhang et al. 2021a]. Given  $n$  points along the ray  $p_i = \mathbf{o} + t\mathbf{v}$  where  $\mathbf{o}$  is the camera origin and  $\mathbf{v}$  is the view direction, we can aggregate these point-wise attributes to obtain the attributes (i.e., depth, normal) of the hit point of the surface as:

$$D_{\text{sdf}} = \sum_{i=0}^n w_i D_i, \mathbf{n}_{\text{sdf}} = \sum_{i=0}^n w_i \mathbf{n}_i \quad (3)$$

where  $w_i$  is the weight of the  $i$ -th point derived from the SDF value.

SDF and NeRF can be unified by NeuS and VolSDF [Wang et al. 2021; Yariv et al. 2021], which maps an SDF value to a density distribution. The distribution in NeuS is defined as:

$$\phi_s(s) = \gamma e^{-\gamma s} / (1 + e^{-\gamma s})^2, \quad (4)$$

where  $s$  is the SDF value and  $\gamma$  is the inverse of standard deviation. Note that  $\gamma$  is a trainable parameter, and  $1/\gamma$  approaches zero as the network training converges.

Among the SDF-based methods, TensoSDF utilizes a tensorial representation for SDF, consisting of a tensorial encoder and MLP decoder, which is formulated as follows:

$$V_p = v_k^X \circ M_k^{YZ} \oplus v_k^Y \circ M_k^{XZ} \oplus v_k^Z \circ M_k^{XY}, s = \Theta(V_p, p), \quad (5)$$

where  $v_k^m$  and  $M_k^{\tilde{m}}$  represent the  $k$ -th vector and matrix factors of their corresponding spatial axes  $m$ , and  $\tilde{m}$  denotes the two axes orthogonal to  $m$  e.g.,  $\tilde{X} = YZ$ .  $\circ$  and  $\oplus$  represent the element-wise multiplication and concatenation operations.  $V_p$  is the latent vector from the tensorial encoder and then is decoded with the position  $p$  by a tiny MLP  $\Theta$  to get the SDF value  $s$ . TensoSDF backbone enables a faster convergence speed and low-cost SDF query.

**Motivation.** The above two representations can both express a 3D scene, where the Gaussian representation is explicit and discontinuous, and the SDF is implicit (or hybrid) and continuous. These two representations lead to different rendering methods: splatting or rasterization for Gaussians and sphere tracing for SDF. While the Gaussian representation significantly boosts the rendering speed to a real-time level, it has difficulties constraining geometries, leading to inferior geometries, as shown in Fig. 2. A straightforward idea is to incorporate these two representations by leveraging the SDF as a prior. However, rendering SDF is time-consuming, which hinders the benefits of 3DGS. Therefore, the essential problem is an elegant incorporation between the Gaussians and the SDF.

### 4 METHOD

In this section, we present our framework GS-ROR for reflective object relighting. First, we present a deferred Gaussian splatting

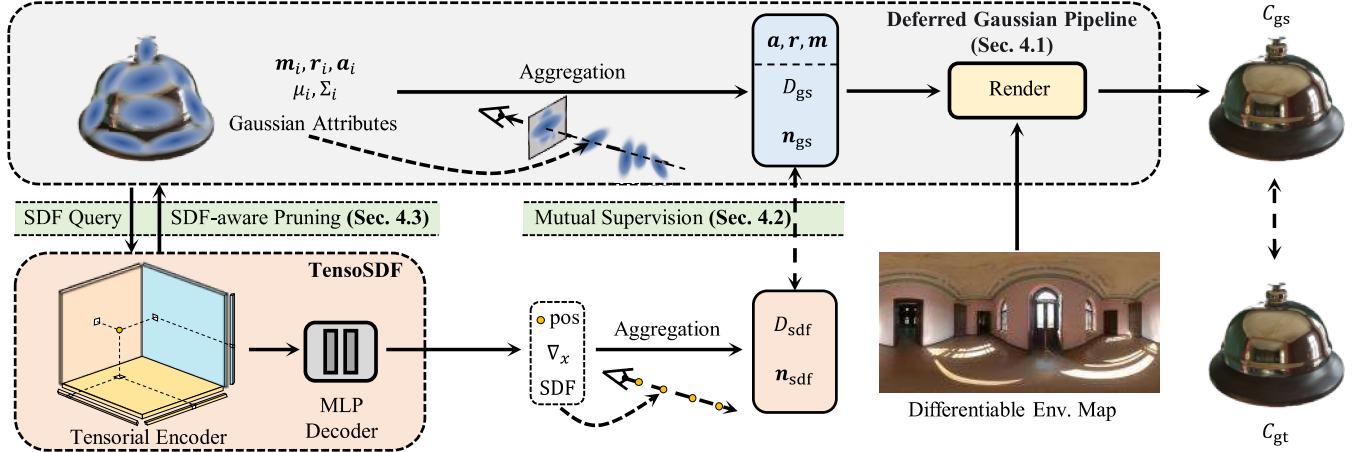


Fig. 3. Overview of our framework. The architecture of our proposed method consists of two geometry representations (*i.e.*, Gaussian primitive and TensoSDF). In the deferred Gaussian pipeline, the shading parameters (*i.e.*, albedo  $\mathbf{a}$ , roughness  $\mathbf{r}$  and metallicity  $\mathbf{m}$ ), normal and depth are projected to the image plane and alpha blended. The pixel color  $C_{gs}$  is calculated using the split-sum approximation and supervised by ground truth color  $C_{gt}$ . In the TensoSDF, we sample rays originated from camera center  $\mathbf{o}$  and view direction  $\mathbf{v}$  and query the SDF value and gradient for each point  $p$  along the ray  $\mathbf{o} + t\mathbf{v}$ . The normal  $\mathbf{n}_{sdf}$  and depth  $D_{sdf}$  are obtained via volume rendering, which is supervised mutually with the normal  $\mathbf{n}_{gs}$  the depth  $D_{gs}$  from Gaussians. Note no color network is used in the SDF part, and only the geometry attributes are volume rendered.

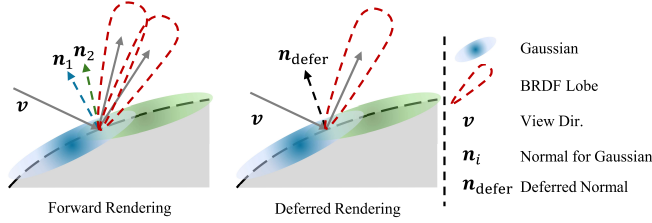


Fig. 4. Two Gaussians with a minor normal difference are overlapped to model an opaque surface. In the forward rendering, the BRDF values are computed w.r.t. to their own normal and are then alpha blended to form the final rendering, which is equivalent to a broader BRDF lobe, leading to a blurry rendering, eventually. In contrast, in the deferred shading, the BRDF is computed w.r.t. the deferred normal, maintaining the sharpness of reflective objects.

for relighting (Sec. 4.1). Then, we introduce the SDF priors into the deferred Gaussian splatting (Sec. 4.2) for geometry regularization. Finally, we propose an SDF-aware pruning strategy to refine the Gaussian distributions (Sec. 4.3).

#### 4.1 Deferred Gaussian splatting for relighting

Starting from GS-IR [Liang et al. 2024], we first construct a forward Gaussian splatting baseline for relighting, using the Disney Principled BDRF model [McAuley et al. 2013] and environment map to model the material and light. We drop the occlusion for efficiency and modify the normal formulation following Gaussian Shader [Jiang et al. 2024] as the combination of the shortest axis direction  $u$  and an offset  $n_\delta$  as  $\mathbf{n} = u + n_\delta$ . The radiance from view  $\mathbf{v}$  for each Gaussian is computed by the split-sum approximation, following previous work [Jiang et al. 2024; Liang et al. 2024], and

then aggregated by alpha blending. With multi-view images as inputs, the reflectance parameters at each Gaussian can be learned, besides the opacity and the environment map, enabling relighting under a novel environment map.

However, this simple Gaussian-based relighting baseline produces blurry relighting results for the reflective surface. The main reason behind this phenomenon is the alpha blending of Gaussians. As shown in Fig. 4, the Gaussians are overlapped to model an opaque surface with slightly different normals. While this difference among Gaussians causes a negligible error for rough objects, it amplifies the BRDF lobe for specular objects, leading to a blurry rendering. The key to addressing this issue is to blend the normals of Gaussians first and then perform shading, *i.e.*, deferred shading.

Specifically, we perform alpha blending on all the attributes (*e.g.*, normal, albedo, roughness) onto the image plane:

$$F = \sum_{i=0}^n f_i \alpha_i \prod_{j=1}^{i-1} (1 - \alpha_j), \quad (6)$$

where  $\alpha_i, \alpha_j$  share the same definition as in Eqn. (2), and  $f_i$  is a attribute of the  $i$ -th Gaussian. Then, we use split-sum approximation to compute the pixel-wise color.

The Gaussians are learned with the following loss function:

$$\mathcal{L}_{gs} = \mathcal{L}_c + \lambda_{nd} \mathcal{L}_{nd} + \lambda_{sm} \mathcal{L}_{sm} + \lambda_m \mathcal{L}_m + \lambda_{\delta n} \mathcal{L}_{\delta n}, \quad (7)$$

where  $\mathcal{L}_c$  is the color supervision between the rendered image and ground truth as in 3DGS,  $\mathcal{L}_{nd}$  is the supervision between the normal from Gaussian and from the estimated depth proposed in Gaussian Shader [Jiang et al. 2024],  $\mathcal{L}_{sm}$  is the smoothness loss for BRDF parameters,  $\mathcal{L}_m$  is the mask loss, and  $\mathcal{L}_{\delta n}$  is the delta normal regularization in Gaussian Shader. More details are shown in Sec. 5.



## 4.2 SDF-aided Gaussian splatting

Thanks to the deferred Gaussian splatting, the blurry issue for reflective object relighting has been addressed. However, the geometry established by Gaussians exhibits erroneous surfaces and floaters, as it tends to overfit the appearance under training light conditions. Hence, more constraints on the geometry are needed. Inspired by NeRO and TensoSDF, we introduce SDF into our framework, as it has shown to be a good prior for geometry regularization. The key is leveraging the capability of SDF while avoiding the expensive rendering. For this, we first choose a performance-friendly backbone for SDF – TensoSDF. Then, we propose geometry-only supervision between Gaussians and SDF, or so-called *mutual supervision*, together with the color supervision between Gaussians renderings and the input images, without any SDF rendering. On the one hand, as Gaussians build the link between rendered images and input images, they can supervise the training of SDF. On the other hand, the SDF can also constrain the Gaussians.

*Mutual supervision.* Even with a performance-friendly SDF backbone, TensoSDF rendering is still expensive, due to the complex color network required to faithfully represent the specular highlights. Therefore, we propose to remove the SDF rendering and connect the SDF and Gaussians with geometry attributes.

Specifically, we pose supervision on the depth and normal of the SDF (Eqn. (3)) from Gaussians (Eqn. (2)):

$$\mathcal{L}_{gs2sdf} = |\mathbf{sg}[D_{gs}] - D_{sdf}| + (1 - \langle \mathbf{sg}[\mathbf{n}_{gs}], \mathbf{n}_{sdf} \rangle), \quad (8)$$

where  $D_{gs}$  and  $D_{sdf}$  are the depth from Gaussians and SDF, respectively,  $\mathbf{n}_{gs}$  and  $\mathbf{n}_{sdf}$  are normals from Gaussians and SDF respectively, and  $\mathbf{sg}[\cdot]$  is the stop-gradient operation.

Besides the above loss, we also utilize the Eikonal loss  $\mathcal{L}_{eik}$ , Hessian loss  $\mathcal{L}_{hes}$ , mask loss  $\mathcal{L}_m$ , and total variance loss  $\mathcal{L}_{tv}$  to regularize the training of SDF, following common practice [Gropp et al. 2020; Li et al. 2024; Zhang et al. 2022c]. The final loss for SDF is

$$\mathcal{L}_{sdf} = \lambda_{gs2sdf} \mathcal{L}_{gs2sdf} + \lambda_{eik} \mathcal{L}_{eik} + \lambda_{hes} \mathcal{L}_{hes} + \mathcal{L}_m + \lambda_{tv} \mathcal{L}_{tv}, \quad (9)$$

where the  $\lambda_{[\cdot]}$  is the corresponding coefficient to adjust the strength of regularization. Among these losses, our proposed  $\mathcal{L}_{gs2sdf}$  enables the optimization of SDF via the geometry of Gaussians, and the  $\mathcal{L}_{eik}$ ,  $\mathcal{L}_{hes}$ ,  $\mathcal{L}_m$ ,  $\mathcal{L}_{tv}$  regularize the SDF to obtain smooth and reasonable geometry.

Then, we design another loss to update Gaussians with SDF priors:

$$\mathcal{L}_{sdf2gs} = |D_{gs} - \mathbf{sg}[D_{sdf}]| + (1 - \langle \mathbf{n}_{gs}, \mathbf{sg}[\mathbf{n}_{sdf}] \rangle). \quad (10)$$

Finally, we obtain the mutual supervision  $\mathcal{L}_{gs2sdf}$  and  $\mathcal{L}_{sdf2gs}$ , which bridges the SDF and Gaussian. Note that the stop-gradient operator is used to differ the strength of the supervisions of both sides.

*Discussion.* In general, SDF is optimized via color supervision between volume-rendered images and input images. However, our loss  $\mathcal{L}_{gs2sdf}$  can optimize the SDF via depth and normal without color supervision, as the depth and the normal are derived from SDF, and thus the gradient from  $\mathcal{L}_{gs2sdf}$  can optimize the SDF. In this way, we can drop the heavy color rendering and optimize the SDF with only geometry attributes (*i.e.*, depth and normal). With other widely used regularizations for SDF (*e.g.*, Eikonal loss), we can obtain a smooth and reasonable geometry from SDF. The loss

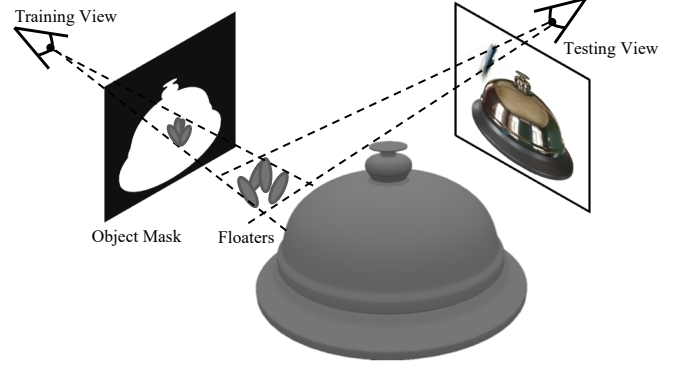


Fig. 5. In this example, the floaters can still be shown in the testing view, even if the mask loss was applied during training. The main reason is that although the floaters are shown outside the mask region in the testing view, they are within the mask region in the training views. Therefore, they can not be masked out by the mask loss.

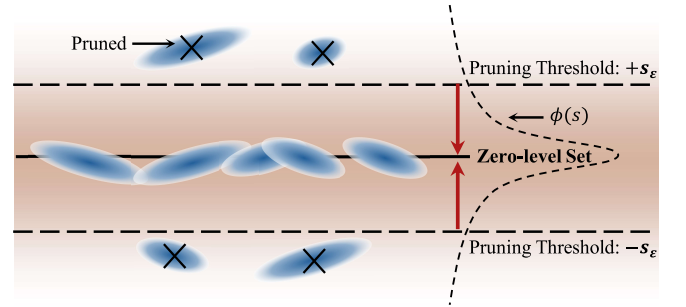


Fig. 6. The illustration of SDF-aware pruning. We define a narrowing threshold, which is adjusted automatically around the zero-level set. The Gaussians out of the threshold will be pruned. This pruning operation ensures all Gaussians are near the surface and avoids the floaters.

$\mathcal{L}_{sdf2gs}$  regularizes the geometry of Gaussians in turn, so we can obtain a better decomposition between geometry and material from the Gaussians.

## 4.3 SDF-aware pruning

With the deferred Gaussians supervised by SDF priors, the geometry becomes smoother. However, we observe some artifacts caused by the overfitting on specular highlights of reflective objects in training views, which leads to Gaussian outliers distant from the surface. These overfitted Gaussians are in the mask region of all training views, so applying the mask loss cannot remove such outliers in training, and we still observe the floaters in the test view, as shown in Fig. 5. Besides, all the above losses supervise the alpha-blended results and lack constraints on individual Gaussians to handle the outliers. Therefore, we propose a Gaussian pruning strategy to enforce the Gaussians close to the zero-level set of SDF. Specifically, for each Gaussian, we check the SDF value at its center and discard the Gaussian if the SDF value is larger than a threshold  $s_\epsilon$ , as shown in the Fig. 6. Since it is laborious to adjust the threshold per scene,

Table 1. Losses used in our paper.

Name	Apply on	Description
$L_c$	GS	Color supervision for 3DGS
$L_{nd}$	GS	Normal Consistency loss from Gaussian Shader.
$L_{sm}$	GS	BRDF smoothness loss from Relightable Gaussian.
$L_{\delta n}$	GS	Normal regularization for Gaussian Shader.
$L_{sdf2gs}$	GS	The proposed depth/normal supervision for GS.
$L_{gs2sdf}$	SDF	The proposed depth/normal supervision for SDF.
$L_{eik}$	SDF	Eikonal loss from Gropp et al. [2020].
$L_{hes}$	SDF	Hessian Loss from Zhang et al. [2022c].
$L_{tv}$	SDF	Total variance loss from TensorRF.
$L_m$	GS/SDF	Mask loss for both 3DGS and SDF.

we link it with the probability density function  $\phi_s(s)$  in Eqn. (4), and the threshold  $s_\epsilon$  can be defined as  $\phi_s(s_\epsilon) = p_t(s_\epsilon > 0)$  in the closed form:

$$s_\epsilon = \gamma \log(2p_t) - \gamma \log\left(\gamma^{-1} - 2p_t - \sqrt{\gamma^{-2} - 4p_t\gamma^{-1}}\right), \quad (11)$$

where  $p_t$  is an empirical hyper-parameter and set to 0.01. In this way, the threshold is determined automatically and narrowed with the SDF in the optimization, so we avoid posing a constant too strict when the surface is under-reconstructed and prune the Gaussians too far away from the surface in the end.

## 5 IMPLEMENTATION DETAILS

This section presents the network structures and the training details.

*Network structures.* The TensoSDF has a resolution of  $400 \times 400$  with feature channels set as 36. The MLP decoder is a two-layer MLP whose width is 128. The Gaussian starts with 100K randomly initialized points.

*Optimization details.* The training of our framework includes three steps. Firstly, the deferred Gaussian splatting without SDF supervision is trained separately for 1K iterations with Eqn. (7) to obtain a coarse geometry. Then, we freeze the Gaussians and warm up the TensoSDF via the depth and normal from Gaussians Eqn. (9) for 3K iterations. Finally, we train the entire framework with a joint loss for 24K iterations:

$$\mathcal{L}_{\text{joint}} = \mathcal{L}_{\text{gs}} + \lambda_{\text{sdf2gs}} \mathcal{L}_{\text{sdf2gs}}. \quad (12)$$

We provide a table of loss functions (see Tab. 1) for better understanding and more details of the losses are in the supplementary material.

We train our model on an NVIDIA RTX 4090 and optimize it with Adam optimizer [Kingma and Ba 2017]. The learning rate for the TensoSDF [Li et al. 2024] grid and the MLP decoder is  $1e^{-2}$  and  $1e^{-3}$ , respectively. The learning rate of Gaussian components follows the setting in 3DGS [Kerbl et al. 2023], and all attributes not in vanilla 3DGS have a learning rate of  $2e^{-3}$ . The initial resolution of TensoSDF is set to 128 and increases to the final resolution  $400 \times 400$ , which uses only 60% capacity of the original TensoSDF, whose final resolution is  $512 \times 512$ . After training, the TensoSDF will be discarded, and only Gaussians will be used for relighting. The pruning threshold is set to 0.01 empirically. The optimization procedure takes about 1.5 hours in total.

## 6 RESULTS

In this section, we describe the evaluation setup (Sec. 6.1), and evaluate our relighting and NVS results (Sec. 6.2). Then, we conduct ablation studies on several main components (Sec. 6.2) and discuss limitations (Sec. 6.4).

### 6.1 Evaluation setup

*Dataset.* We evaluate our method on three synthetic datasets and one real-scene dataset. We utilize the TensoIR [Jin et al. 2023] synthetic and Glossy Blender dataset [Liu et al. 2023] to evaluate the performance of diffuse and specular materials, respectively. Besides, we use the Shiny Blender dataset to show the generalization ability of our method for diverse materials. For real scenes, we select some specular objects from the NeLF++ [Zhang et al. 2023].

*Methods for comparison.* We select 7 representative methods for comparison. We choose MII [Zhang et al. 2022b], TensoIR [Jin et al. 2023], TensoSDF [Li et al. 2024], and NeRO [Liu et al. 2023] for NeRF-based methods and Gaussian Shader [Jiang et al. 2024], GS-IR [Liang et al. 2024], and Relightable Gaussian [Gao et al. 2024] for Gaussian-based methods. We trained these models based on their public codes and configurations. Note that we add the mask loss to train all the compared methods, for stabilizing training and fair comparison.

*Metrics.* We use the peak signal-to-noise ratio (PSNR) and structural similarity index (SSIM) [Wang et al. 2004] to measure the quality of results for the comparison and ablation study in the main paper. We present the learned perceptual image patch similarity (LPIPS) [Zhang et al. 2018] in the supplementary materials. Due to the ambiguity between albedo and light, we normalize the relighting images to match the average colors of ground-truth images before computing the metrics, following NeRO. When the ground truth albedo is available, we rescale the relighting images based on the ground truth albedo and predicted albedo, following TensoIR. We record the mean training time and the frame per second (FPS)<sup>1</sup> in the evaluation, which tests on a single RTX 4090.

### 6.2 Comparison with previous works

*Relighting of reflective objects.* We evaluate the relighting performance of specular materials on the Glossy Blender dataset. The quantitative measurements are shown in Tab. 2, and the relighting visualizations are placed in Fig. 10. Our method outperforms other Gaussian-based methods and achieves competitive results of the NeRF-based methods. We also show the decomposed maps in Fig. 11 and Fig. 12. Due to the SDF priors and the deferred Gaussian pipeline, our method can produce a smooth surface without losing details and predict reasonable BRDF parameters.

*Relighting of diffuse objects.* Although our design focuses on reflective surfaces, it can also show benefits for diffuse objects. We validate our method on the TensoIR dataset. The quantitative measurements are shown in Tab. 3. The comparison with NeRF-based

<sup>1</sup>NeRO and TensoSDF use the Cycles Render Engine in Blender to provide relighting results, so the FPS depends on samples per pixel, which is 1024 following the NeRO setting.

Table 2. Relighting quality in terms of PSNR $\uparrow$  and SSIM $\uparrow$  on the Blender Glossy dataset. Numbers in **bold** indicate the best performance, and underscored numbers indicate the second best. Our method outperforms existing Gaussian-based methods. Note that although our quantitative metrics are lower than some NeRF-based methods, our training time is much shorter (25% of TensoSDF, 13% of NeRO).

	NeRF-based				Gaussian-based			
	MII PSNR/SSIM	TensoIR PSNR/SSIM	TensoSDF PSNR/SSIM	NeRO PSNR/SSIM	GShader PSNR/SSIM	GS-IR PSNR/SSIM	RelightGS PSNR/SSIM	Ours PSNR/SSIM
Angel	16.24/.8236	10.24/.2238	<u>20.40/.8969</u>	16.21/.7819	17.49/.8336	15.64/.6126	16.65/.8013	<b>20.81/.8775</b>
Bell	17.41/.8594	10.11/.1018	<u>29.91/.9767</u>	<b>31.19/.9794</b>	19.01/.8804	12.61/.2807	16.15/.8391	24.49/.9267
Cat	17.68/.8521	9.10/.1644	26.12/.9354	<b>28.42/.9579</b>	16.00/.8642	18.04/.7907	17.49/.8503	<u>26.28/.9421</u>
Horse	20.98/.8997	10.42/.1931	<b>27.18/.9567</b>	<u>25.56/.9437</u>	22.49/.9262	17.40/.7270	20.63/.8832	<u>23.31/.9376</u>
Luyu	17.89/.8050	8.27/.2375	19.91/.8825	<b>26.22/.9092</b>	15.62/.8254	19.00/.7727	17.47/.8168	<u>22.61/.8995</u>
Potion	17.13/.8094	6.21/.0846	<u>27.71/.9422</u>	<b>30.14/.9561</b>	12.33/.7575	16.37/.7051	14.99/.7799	<u>25.67/.9175</u>
Tbell	16.54/.8262	7.47/.1609	<u>23.33/.9404</u>	<b>25.45/.9607</b>	14.42/.8007	14.35/.5419	15.99/.7965	22.80/.9180
Teapot	16.71/.8546	9.96/.2093	<u>25.16/.9482</u>	<b>29.87/.9755</b>	18.21/.8560	16.63/.7646	17.36/.8389	21.17/.8932
Mean	17.57/.8413	8.97/.1719	<u>24.97/.9349</u>	<b>26.63/.9331</b>	16.95/.8430	16.26/.6494	17.09/.8258	23.39/.9140
Training Time	4h	5h	6h	12h	0.5h	0.5h	1h	1.5h
Ren. Time (FPS)	1/30	1/60	1/4	1/4	50	214	1.5	208

Table 3. Relighting quality in terms of PSNR $\uparrow$  and SSIM $\uparrow$  on the TensoIR synthetic dataset. Numbers in **bold** indicate the best performance, and underscored numbers indicate the second best.

	GShader PSNR/SSIM	GS-IR PSNR/SSIM	RelightGS PSNR/SSIM	Ours PSNR/SSIM
Armad.	22.86/.9280	27.65/.9078	<u>30.76/.9526</u>	<b>31.33/.9593</b>
Ficus	24.61/.9491	23.63/.8662	<b>27.23/.9637</b>	<u>26.28/.9542</u>
Hotdog	17.45/.8838	21.51/.8853	<u>24.59/.9162</u>	<b>25.21/.9307</b>
Lego	13.41/.7904	<u>22.88/.8342</u>	22.49/.8682	<b>25.46/.9083</b>
Mean	19.58/.8878	23.92/.8734	<u>26.27/.9252</u>	<b>27.07/.9381</b>

methods and relighting visualizations are in the supplementary material. Our methods can outperform the existing Gaussian-based methods and some NeRF-based methods on the TensoIR dataset, which reveals the robustness under diverse materials.

*Relighting on real data.* For real scenes, we select some objects with specular highlights from NeLF++ [Zhang et al. 2023], and the results are shown in Fig. 13. As there is no available ground truth, we only show the reference training views and some results under novel light conditions. Our method produces reasonable relighting results under novel lighting. Besides, our method achieves a balance between quality and training speed, enabling reflective surface modeling with only 25% training time of TensoSDF and 13% of NeRO. Our method supports real-time rendering with 200+ FPS, much faster than all NeRF-based and some Gaussian-based methods.

*NVS.* We also present the NVS results on the Glossy Blender dataset and the Shiny Blender Dataset. The quantitative evaluation in terms of PSNR and SSIM is present in Tabs. 4 and 5. Our method can provide high-quality NVS results with sharper highlights, which are present in Figs. 14 and 15, revealing the wide applications of

Table 4. NVS quality in terms of PSNR $\uparrow$  and SSIM $\uparrow$  on the Glossy Blender dataset. Numbers in **bold** indicate the best performance, and underscored numbers indicate the second best.

	GS-IR PSNR/SSIM	RelightGS PSNR/SSIM	GShader PSNR/SSIM	Ours PSNR/SSIM
Angel	20.77/.6935	23.12/.7841	<u>27.14/.9226</u>	<b>29.32/.9445</b>
Bell	19.05/.4895	24.38/.8952	<u>30.00/.9409</u>	<b>31.53/.9694</b>
Cat	27.91/.9075	29.73/.9487	<u>31.25/.9604</u>	<b>31.72/.9672</b>
Horse	20.85/.6835	22.88/.7769	<u>26.03/.9314</u>	<b>27.09/.9479</b>
Luyu	24.96/.8637	25.97/.8986	<u>27.35/.9175</u>	<b>28.53/.9383</b>
Potion	25.81/.8217	29.03/.9277	<u>29.53/.9357</u>	<b>30.51/.9503</b>
Tbell	20.72/.6193	23.03/.8878	<u>23.86/.9031</u>	<b>29.48/.9648</b>
Teapot	20.56/.8427	20.82/.8719	<u>23.56/.8986</u>	<b>26.41/.9468</b>
Mean	22.58/.6322	24.87/.8739	<u>27.34/.9263</u>	<b>29.32/.9537</b>

our method. Our method outperforms the existing Gaussian-based

Table 5. NVS quality with Gaussian-based methods on Shiny Blender dataset in terms of PSNR $\uparrow$  and SSIM $\uparrow$ . Numbers in **bold** indicate the best performance, and underscored numbers indicate the second best.

	GS-IR PSNR/SSIM	RelightGS PSNR/SSIM	GShader PSNR/SSIM	Ours PSNR/SSIM
Ball	18.30/.7584	21.39/.9047	<u>30.40/.9623</u>	<b>35.50/.9849</b>
Car	25.30/.8867	26.59/.9267	<u>28.39/.9388</u>	<b>30.52/.9638</b>
Coffee	30.72/.9463	<b>32.57/.9710</b>	<u>30.79/.9690</u>	29.64/.9568
Helmet	25.08/.9018	26.95/.9469	<u>28.78/.9549</u>	<b>32.62/.9738</b>
Teapot	38.21/.9900	<u>43.86/.9963</u>	43.35/.9957	<b>43.88/.9964</b>
Toaster	18.66/.7418	20.07/.8745	<u>23.95/.9130</u>	<b>25.89/.9379</b>
Mean	26.05/.8708	28.57/.9367	<u>30.94/.9556</u>	<b>33.01/.9689</b>

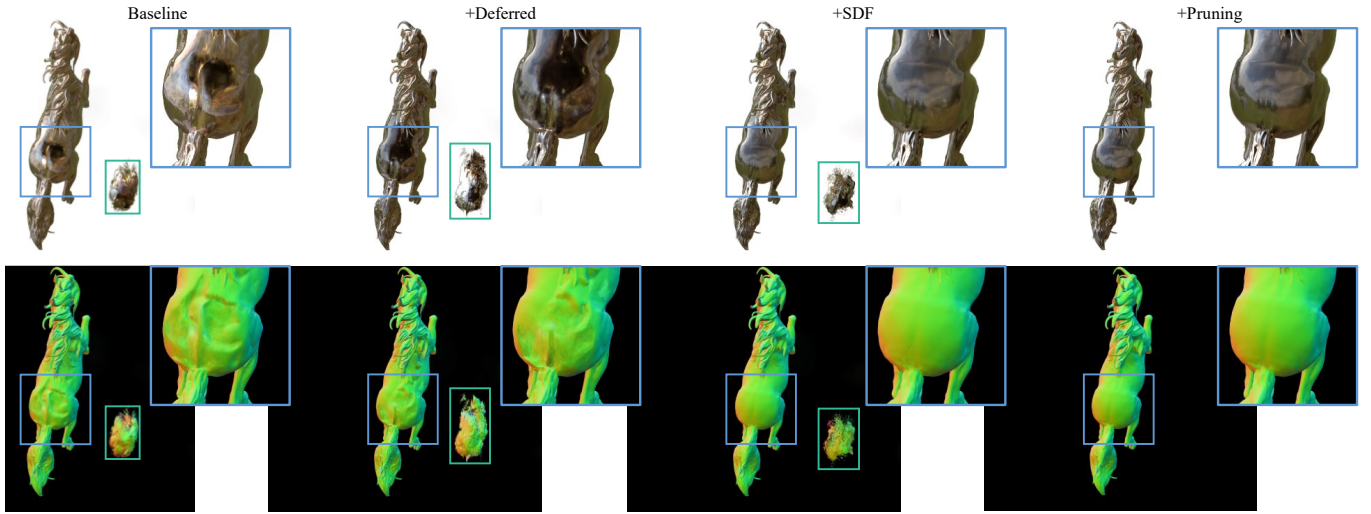


Fig. 7. Ablation of several key components in our method, including the deferred shading, SDF supervision and pruning. The insets are shown in blue, and some floaters are shown in green.

methods on most scenes. However, our method fails in the Coffee scene, as the deferred pipeline assumes an opaque surface, and the liquid in the Coffee does not meet the assumption. Besides, we present a comparison of normal estimation in Fig. 16 and the mean angular error (MAE) in Tab. 6. Thanks to the SDF priors, our method can provide robust normal estimation, while the results of other Gaussian-based methods are overfitted or noisy.

Table 6. Normal quality with Gaussian-based methods on Shiny Blender dataset in terms of MAE $\downarrow$ .

	GS-IR	RelightGS	GShader	Ours
Ball	25.79	22.44	<u>7.03</u>	<b>0.92</b>
Car	28.31	26.02	<u>14.05</u>	<b>11.98</b>
Coffee	15.38	<u>13.39</u>	14.93	<b>12.24</b>
Helmet	25.58	19.63	<u>9.33</u>	<b>4.10</b>
Teapot	15.35	9.21	<u>7.17</u>	<b>5.88</b>
Toaster	33.51	28.17	<u>13.08</u>	<b>8.24</b>
Mean	23.99	19.81	<u>10.93</u>	<b>7.23</b>

### 6.3 Ablation study

We conduct ablation studies on the key components of our model on the Glossy Blender dataset. The mean relighting PSNR and SSIM are presented in the Tab. 8. We can see a consistent improvement when we employ new components to the model. We start from a baseline that first computes colors for Gaussians and alpha blends them as in 3DGS. As shown in the 1st column in Fig. 7, the baseline cannot render a reflective surface and provide the result with obvious artifacts due to the blending issue discussed in Sec. 4.1.

*Deferred Gaussian pipeline.* After applying the deferred Gaussian pipeline, this variant provides a more specular result. However, due to the erroneous normal, the surface reflects light from the wrong

directions, shown in the 2nd column of Fig. 7. We observe more artifacts from the deferred results, for the pixel color from deferred shading corresponds to one shading point on the estimated surface while the one from forward shading is a combination of rendered colors of multiple Gaussians. The deferred formulation leaves less freedom for individual Gaussians to overfit. Consequently, more Gaussian outliers are generated to overfit sharp highlights, causing additional artifacts. Nevertheless, the deferred shading is necessary for specular materials (Sec. 4.1), and its issue has been solved in our full model.

*TensoSDF incorporation.* Then, we incorporate the TensoSDF and utilize its priors to regularize the geometry. The model without TensoSDF is vulnerable to the local minima and overfits under the training light condition, leading to erroneous geometry estimation. After employing the TensoSDF (3rd column in Fig. 7), the model mitigates the ambiguity between material and geometry and predicts a reasonable normal. We also validate the effectiveness of our mutual supervision by comparing it to supervision by a pretrained TensoSDF. As shown in Tab. 7, although using the pretrained TensoSDF for supervision could improve the quality slightly, it needs 5 hours for TensoSDF training. In contrast, our method achieves a balance between performance and efficiency. Besides, our method preserves the details while SDF-based methods fail, as shown in Fig. 8 (see the cat whisker), revealing the benefits of our Gaussian representation.

*SDF-aware pruning.* Eventually, we apply the SDF-aware pruning operation to our model. The models without pruning are likely to overfit under training views, and we can observe some unnecessary Gaussians under test views, causing severe floaters. Note that the overfitted Gaussians are invisible and in the mask region in training views. Therefore, we still observe the floater in the testing views, even though we apply the mask loss during training. After applying pruning, all Gaussians are located near the surface at the end of the



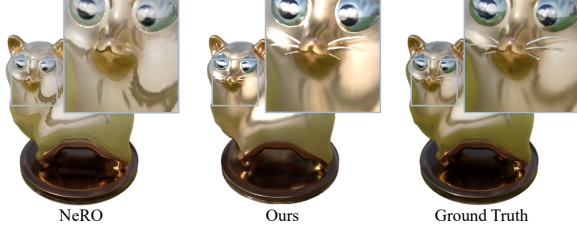


Fig. 8. Our method preserves the details that are lost in the SDF-based method (i.e., NeRO), revealing the benefits of the Gaussian representation.

Table 7. Comparison of the relighting quality between mutual supervision (Ours) and using a pretrained TensoSDF to supervise Gaussians unidirectionally on the Glossy Blender dataset. Despite the slight quality improvement, using the pretrained model leads to an extensive training time cost.

	Angel	Cat	Horse
Ours	20.81	26.28	23.31
Pretrained	21.45 (+0.64/+5h)	26.37 (+0.09/+5h)	24.59 (+1.28/+5h)

Table 8. Ablation study of three key components on the Glossy Blender dataset. “Def.” means the deferred Gaussian pipeline, “Inc.” means the incorporation of SDF and Gaussian, and “Pru.” means the pruning operation.

Components			Scene		
Def.	Inc.	Pru.	Horse PSNR/SSIM	Cat PSNR/SSIM	Angel PSNR/SSIM
			20.33/0.9012	24.18/0.9253	18.86/0.8562
✓			20.59/0.9089	24.87/0.9323	18.86/0.8574
✓	✓		23.12/0.9357	26.22/0.9417	20.48/0.8793
✓	✓	✓	<b>23.31/0.9376</b>	<b>26.28/0.9421</b>	<b>20.81/0.8775</b>

training, and the model provides relighting results without floater, as shown in the 4th column in Fig. 7.

#### 6.4 Discussion and limitations

Our model improves the relighting quality compared to other Gaussian-based methods. However, some issues remain to be solved. The SDF representation used in our framework is used as a prior, and it can not be used for exporting a faithful mesh due to its low resolution. Besides, we observe the split-sum approximation in DiffRast [Laine et al. 2020] causes blurry renderings for extremely low-roughness surfaces. We render a mirror-like plane using the Cycle path-tracing renderer in Blender and the split-sum approximation in the DiffRast. The comparison is in Fig. 9, and the split-sum result is blurry. We believe replacing it with a more accurate rendering method will improve the relighting quality. Last, we only consider direct lighting in our framework, and introducing indirect illumination will benefit the relighting quality. We leave it for future work.

## 7 CONCLUSION

In this paper, we present a novel framework for real-time reflective object inverse rendering. We design an SDF-aided Gaussian splatting framework, using the mutual supervision of the depth and normal

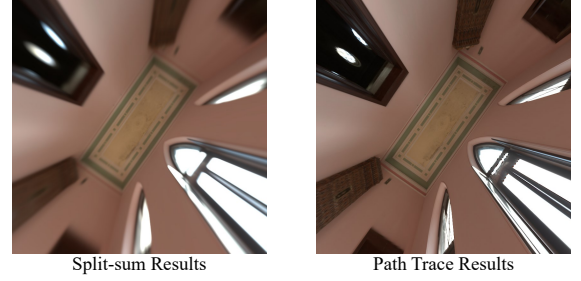


Fig. 9. The comparison between the result using Cycle path-tracing renderer in Blender and the one using split-sum approximation in DiffRast. The split-sum result is blurry with extremely low roughness.

between deferred Gaussians and SDF to improve the quality of geometry from Gaussians. Besides, we propose an SDF-aware pruning strategy with an automatically adjusted threshold, regularizing the position of Gaussian and avoiding the floater artifact. Consequently, our method outperforms the existing Gaussian-based inverse rendering methods without losing efficiency. It is competitive with the NeRF-based methods in terms of quality, with much less training and rendering time. In future work, extending our framework to complex scenarios with multiples objects is a potential direction.

## REFERENCES

- Jonathan T. Barron, Ben Mildenhall, Matthew Tancik, Peter Hedman, Ricardo Martin-Brualla, and Pratul P. Srinivasan. 2021. Mip-NeRF: A Multiscale Representation for Anti-Aliasing Neural Radiance Fields. In *ICCV*. IEEE, New York, NY, USA, 5855–5864.
- Jonathan T. Barron, Ben Mildenhall, Dor Verbin, Pratul P. Srinivasan, and Peter Hedman. 2022. Mip-NeRF 360: Unbounded Anti-Aliased Neural Radiance Fields. In *CVPR*. IEEE, New York, NY, USA, 5470–5479.
- Sai Bi, Zexiang Xu, Pratul Srinivasan, Ben Mildenhall, Kalyan Sunkavalli, Miloš Hašan, Yannick Hold-Geoffroy, David Kriegman, and Ravi Ramamoorthi. 2020. Neural Reflectance Fields for Appearance Acquisition. arXiv:2008.03824
- Mark Boss, Raphael Braun, Varun Jampani, Jonathan T. Barron, Ce Liu, and Hendrik P.A. Lensch. 2021a. NeRD: Neural Reflectance Decomposition From Image Collections. In *ICCV*. IEEE, New York, NY, USA, 12684–12694.
- Mark Boss, Varun Jampani, Raphael Braun, Ce Liu, Jonathan Barron, and Hendrik P.A. Lensch. 2021b. Neural-PIL: Neural Pre-Integrated Lighting for Reflectance Decomposition. In *NeurIPS*, M. Ranzato, A. Beygelzimer, Y. Dauphin, P.S. Liang, and J. Wortman Vaughan (Eds.), Vol. 34. Curran Associates, Inc., Red Hook, NY, USA, 10691–10704.
- Anpei Chen, Zexiang Xu, Andreas Geiger, Jingyi Yu, and Hao Su. 2022. TensoRF: Tensorial Radiance Fields. In *ECCV*. Springer, Berlin, Heidelberg, 333–350. [https://doi.org/10.1007/978-3-031-19824-3\\_20](https://doi.org/10.1007/978-3-031-19824-3_20)
- Hanlin Chen, Chen Li, and Gim Hee Lee. 2023. NeuSG: Neural Implicit Surface Reconstruction with 3D Gaussian Splatting Guidance. arXiv:2312.00846
- Pinxuan Dai, Jiamin Xu, Wenxiang Xie, Xinguo Liu, Huamin Wang, and Weiwei Xu. 2024. High-quality Surface Reconstruction using Gaussian Surfels. In *SIGGRAPH (SIGGRAPH '24)*. Association for Computing Machinery, New York, NY, USA, Article 22, 11 pages. <https://doi.org/10.1145/3641519.3657441>
- Sara Fridovich-Keil, Alex Yu, Matthew Tancik, Qinhong Chen, Benjamin Recht, and Angjoo Kanazawa. 2022. Plenoxels: Radiance Fields Without Neural Networks. In *CVPR*. IEEE, New York, NY, USA, 5501–5510.
- Jian Gao, Chun Gu, Youtian Lin, Zhihao Li, Hao Zhu, Xun Cao, Li Zhang, and Yao Yao. 2024. Relightable 3D Gaussians: Realistic Point Cloud Relighting with BRDF Decomposition and Ray Tracing. arXiv:2311.16043
- Amos Gropp, Lior Yariv, Niv Haim, Matan Atzmon, and Yaron Lipman. 2020. Implicit geometric regularization for learning shapes. In *ICML (ICML '20)*. JMLR.org, Article 355, 11 pages.
- Antoine Guédon and Vincent Lepetit. 2024. SuGar: Surface-Aligned Gaussian Splatting for Efficient 3D Mesh Reconstruction and High-Quality Mesh Rendering. In *CVPR*. IEEE, New York, NY, USA, 5354–5363.
- Binbin Huang, Zehao Yu, Anpei Chen, Andreas Geiger, and Shenghua Gao. 2024. 2D Gaussian Splatting for Geometrically Accurate Radiance Fields. In *SIGGRAPH (SIGGRAPH '24)*. Association for Computing Machinery, New York, NY, USA, Article

- 32, 11 pages. <https://doi.org/10.1145/3641519.3657428>
- Yingwenqi Jiang, Jiadong Tu, Yuan Liu, Xifeng Gao, Xiaoxiao Long, Wenping Wang, and Yuexin Ma. 2024. GaussianShader: 3D Gaussian Splatting with Shading Functions for Reflective Surfaces. In *CVPR*. IEEE, New York, NY, USA, 5322–5332.
- Haian Jin, Isabella Liu, Peijia Xu, Xiaoshuai Zhang, Songfang Han, Sai Bi, Xiaowei Zhou, Zexiang Xu, and Hao Su. 2023. TensorIR: Tensorial Inverse Rendering. In *CVPR*. IEEE, New York, NY, USA, 165–174.
- Bernhard Kerbl, Georgios Kopanas, Thomas Leimkühler, and George Drettakis. 2023. 3D Gaussian Splatting for Real-Time Radiance Field Rendering. *ACM TOG* 42, 4 (2023), 139–1.
- Diederik P. Kingma and Jimmy Ba. 2017. Adam: A Method for Stochastic Optimization. arXiv:1412.6980
- Samuli Laine, Janne Hellsten, Tero Karras, Yeongho Seol, Jaakko Lehtinen, and Timo Aila. 2020. Modular primitives for high-performance differentiable rendering. *ACM TOG* 39, 6, Article 194 (November 2020), 14 pages. <https://doi.org/10.1145/3414685.3417861>
- Jia Li, Lu Wang, Lei Zhang, and Beibei Wang. 2024. TensoSDF: Roughness-aware Tensorial Representation for Robust Geometry and Material Reconstruction. *ACM TOG* 43, 4, Article 150 (July 2024), 13 pages. <https://doi.org/10.1145/3658211>
- Zhaoshuo Li, Thomas Müller, Alex Evans, Russell H. Taylor, Mathias Unberath, Ming-Yu Liu, and Chen-Hsuan Lin. 2023. Neuralangelo: High-Fidelity Neural Surface Reconstruction. In *CVPR*. IEEE, New York, NY, USA, 8456–8465.
- Zhihao Liang, Qi Zhang, Ying Feng, Ying Shan, and Kui Jia. 2024. GS-IR: 3D Gaussian Splatting for Inverse Rendering. In *CVPR*. IEEE, New York, NY, USA, 21644–21653.
- Jingwang Ling, Ruihan Yu, Feng Xu, Chun Du, and Shuang Zhao. 2024. NeRF as a Non-Distant Environment Emitter in Physics-based Inverse Rendering. In *SIGGRAPH (SIGGRAPH '24)*. Association for Computing Machinery, Denver, CO, USA, Article 39, 12 pages. <https://doi.org/10.1145/3641519.3657404>
- Yuan Liu, Peng Wang, Cheng Lin, Xiaoxiao Long, Jiepeng Wang, Lingjie Liu, Taku Komura, and Wenping Wang. 2023. NeRO: Neural Geometry and BRDF Reconstruction of Reflective Objects from Multiview Images. *ACM TOG* 42, 4, Article 114 (July 2023), 22 pages. <https://doi.org/10.1145/3592134>
- Li Ma, Vasu Agrawal, Haithem Turki, Changil Kim, Chen Gao, Pedro Sander, Michael Zollhöfer, and Christian Richardt. 2024. SpecNeRF: Gaussian Directional Encoding for Specular Reflections. arXiv:2312.13102
- Stephen McAuley, Stephen Hill, Adam Martinez, Ryusuke Villemin, Matt Pettineo, Dimitar Lazarov, David Neubelt, Brian Karis, Christophe Hery, Naty Hoffman, and Hakan Zap Andersson. 2013. Physically based shading in theory and practice. In *ACM SIGGRAPH 2013 Courses (SIGGRAPH '13)*. Association for Computing Machinery, New York, NY, USA, Article 22, 8 pages. <https://doi.org/10.1145/2504435.2504457>
- Ben Mildenhall, Pratul P. Srinivasan, Matthew Tancik, Jonathan T. Barron, Ravi Ramamoorthi, and Ren Ng. 2020. NeRF: Representing Scenes as Neural Radiance Fields for View Synthesis. In *ECCV*. Springer, Berlin, Heidelberg, 405–421.
- Thomas Müller, Alex Evans, Christoph Schied, and Alexander Keller. 2022. Instant neural graphics primitives with a multiresolution hash encoding. *ACM TOG* 41, 4, Article 102 (July 2022), 15 pages. <https://doi.org/10.1145/3528223.3530127>
- Radu Alexandru Rosu and Sven Behnke. 2023. PermutoSDF: Fast Multi-View Reconstruction With Implicit Surfaces Using Permutohedral Lattices. In *CVPR*. IEEE, New York, NY, USA, 8466–8475.
- Yahao Shi, Yanmin Wu, Chenming Wu, Xing Liu, Chen Zhao, Haocheng Feng, Jingtuo Liu, Liangjun Zhang, Jian Zhang, Bin Zhou, Errui Ding, and Jingdong Wang. 2023. GIR: 3D Gaussian Inverse Rendering for Relightable Scene Factorization. arXiv:2312.05133
- Pratul P. Srinivasan, Boyang Deng, Xiuming Zhang, Matthew Tancik, Ben Mildenhall, and Jonathan T. Barron. 2021. NeRV: Neural Reflectance and Visibility Fields for Relighting and View Synthesis. In *CVPR*. IEEE, New York, NY, USA, 7495–7504.
- Dor Verbin, Peter Hedman, Ben Mildenhall, Todd Zickler, Jonathan T. Barron, and Pratul P. Srinivasan. 2022. Ref-NeRF: Structured View-Dependent Appearance for Neural Radiance Fields. In *CVPR*. IEEE, New York, NY, USA, 5491–5500.
- Haoyuan Wang, Wenbo Hu, Lei Zhu, and Rynson W.H. Lau. 2024. Inverse Rendering of Glossy Objects via the Neural Plenoptic Function and Radiance Fields. In *CVPR*. IEEE, New York, NY, USA, 19999–20008.
- Peng Wang, Lingjie Liu, Yuan Liu, Christian Theobalt, Taku Komura, and Wenping Wang. 2021. NeuS: Learning Neural Implicit Surfaces by Volume Rendering for Multi-view Reconstruction. In *NeurIPS*, M. Ranzato, A. Beygelzimer, Y. Dauphin, P.S. Liang, and J. Wortman Vaughan (Eds.), Vol. 34. Curran Associates, Inc., Red Hook, NY, USA, 27171–27183.
- Zhou Wang, A.C. Bovik, H.R. Sheikh, and E.P. Simoncelli. 2004. Image quality assessment: from error visibility to structural similarity. *IEEE TIP* 13, 4 (2004), 600–612.
- Zixiong Wang, Yunxiao Zhang, Rui Xu, Fan Zhang, Peng-Shuai Wang, Shuangmin Chen, Shiqing Xin, Wenping Wang, and Changhe Tu. 2023. Neural-Singular-Hessian: Implicit Neural Representation of Unoriented Point Clouds by Enforcing Singular Hessian. *ACM TOG* 42, 6, Article 274 (December 2023), 14 pages. <https://doi.org/10.1145/3618311>
- Tong Wu, Jia-Mu Sun, Yu-Kun Lai, Yuewen Ma, Leif Kobbelt, and Lin Gao. 2024. DeferredGS: Decoupled and Editable Gaussian Splatting with Deferred Shading. Ziyi Yang, Yanzhen Chen, Xinyu Gao, Yazhen Yuan, Yu Wu, Xiaowei Zhou, and Xiaogang Jin. 2023. SiRe-IR: Inverse Rendering for BRDF Reconstruction with Shadow and Illumination Removal in High-Illuminance Scenes. arXiv:2310.13030
- Ziyi Yang, Xinyu Gao, Yangtian Sun, Yihua Huang, Xiaoyang Lyu, Wen Zhou, Shaohui Jiao, Xiaojuan Qi, and Xiaogang Jin. 2024. Spec-Gaussian: Anisotropic View-Dependent Appearance for 3D Gaussian Splatting. arXiv:2402.15870
- Lior Yariv, Jiatao Gu, Yoni Kasten, and Yaron Lipman. 2021. Volume Rendering of Neural Implicit Surfaces. In *NeurIPS*, M. Ranzato, A. Beygelzimer, Y. Dauphin, P.S. Liang, and J. Wortman Vaughan (Eds.), Vol. 34. Curran Associates, Inc., Red Hook, NY, USA, 4805–4815.
- Keyang Ye, Qiming Hou, and Kun Zhou. 2024. 3D Gaussian Splatting with Deferred Reflection. In *SIGGRAPH (SIGGRAPH '24)*. Association for Computing Machinery, New York, NY, USA, Article 40, 10 pages. <https://doi.org/10.1145/3641519.3657456>
- Ze-Xin Yin, Jiaxiong Qiu, Ming-Ming Cheng, and Bo Ren. 2023. Multi-Space Neural Radiance Fields. In *CVPR*. IEEE, New York, NY, USA, 12407–12416.
- Mulin Yu, Tao Lu, Linning Xu, Lihan Jiang, Yuanbo Xiangli, and Bo Dai. 2024. GSDF: 3DGS Meets SDF for Improved Rendering and Reconstruction. arXiv:2311.16473
- Jingyang Zhang, Yao Yao, Shiwei Li, Tian Fang, David McKinnon, Yanghai Tsin, and Long Quan. 2022c. Critical Regularizations for Neural Surface Reconstruction in the Wild. In *CVPR*. IEEE, New York, NY, USA, 6270–6279.
- Jingyang Zhang, Yao Yao, Shiwei Li, Jingbo Liu, Tian Fang, David McKinnon, Yanghai Tsin, and Long Quan. 2023. NeLLF++: Inter-Reflectable Light Fields for Geometry and Material Estimation. In *ICCV*. IEEE, New York, NY, USA, 3601–3610.
- Kai Zhang, Fujun Luan, Zhengqi Li, and Noah Snavely. 2022a. IRON: Inverse Rendering by Optimizing Neural SDFs and Materials From Photometric Images. In *CVPR*. IEEE, New York, NY, USA, 5565–5574.
- Kai Zhang, Fujun Luan, Qianqian Wang, Kavita Bala, and Noah Snavely. 2021a. PhysSG: Inverse Rendering With Spherical Gaussians for Physics-Based Material Editing and Relighting. In *CVPR*. IEEE, New York, NY, USA, 5453–5462.
- Richard Zhang, Phillip Isola, Alexei A. Efros, Eli Shechtman, and Oliver Wang. 2018. The Unreasonable Effectiveness of Deep Features as a Perceptual Metric. In *CVPR*. IEEE, New York, NY, USA, 10.
- Xiuming Zhang, Pratul P. Srinivasan, Boyang Deng, Paul Debevec, William T. Freeman, and Jonathan T. Barron. 2021b. NeRFactor: neural factorization of shape and reflectance under an unknown illumination. *ACM TOG* 40, 6, Article 237 (dec 2021), 18 pages.
- Yuanqing Zhang, Jiaming Sun, Xingyi He, Huan Fu, Rongfei Jia, and Xiaowei Zhou. 2022b. Modeling Indirect Illumination for Inverse Rendering. In *CVPR*. IEEE, New York, NY, USA, 18643–18652.

# Supplementary Material – GS-ROR: 3D Gaussian Splatting for Reflective Object Relighting via SDF Priors

## 1 LOSS DETAILS

We introduce the definition and weights of losses we used in the main paper. The color loss is defined as in 3DGS [Kerbl et al. 2023]

$$L_c = \lambda \|C_{gs} - C_{gt}\|_1 + (1 - \lambda)(1 - \text{SSIM}(C_{gs}, C_{gt})), \quad (1)$$

where  $C_{gs}$  is the rendered color from Gaussians and  $C_{gt}$  is the ground truth color. The coefficient  $\lambda$  is set to 0.8. The supervision  $L_{nd}$  from normal is defined as

$$L_{nd} = \|\hat{\mathbf{n}} - \mathbf{n}\|^2, \quad (2)$$

where  $\hat{\mathbf{n}}, \mathbf{n}$  are the normal from depth and the normal from Gaussians, respectively. Our normal formulation follows Gaussian Shader, which combines the shortest axis and a learnable residual [Jiang et al. 2024] as

$$\mathbf{n} = u + n_\delta, \quad (3)$$

where  $u$  is the shortest axis and  $n_\delta$  is the residual term. To prevent the residual from dominating the normal direction, we add a penalty to it:

$$L_{\delta_n} = \|n_\delta\|^2. \quad (4)$$

The smoothness loss for BRDF parameters (*i.e.*, albedo  $\mathbf{a}$ , roughness  $\mathbf{r}$ , metallicity  $\mathbf{m}$ ) is defined as

$$L_{sm} = \|\nabla f\| \exp^{-\|\nabla C_{gt}\|}, (f \in \{\mathbf{a}, \mathbf{r}, \mathbf{m}\}) \quad (5)$$

where  $\nabla$  is the gradient operator and  $C_{gt}$  is the color of ground-truth image. The mask loss is the binary cross entropy between predicted and ground-truth masks.

In the first phase, we set the corresponding weights  $\lambda_{[\cdot]}$  as  $\lambda_{nd} = 0.2$ ,  $\lambda_{sm} = 1e^{-2}$ ,  $\lambda_m = 0.2$ ,  $\lambda_{\delta_n} = 1e^{-3}$ . In the second phase, the loss weights are set as  $\lambda_{gs2sdf} = 0.5$ ,  $\lambda_{eik} = 0.1$ ,  $\lambda_{hes} = 5e^{-4}$ ,  $\lambda_{tv} = 0.1$ . In third phase, the loss weights are set as  $\lambda_{sdf2gs} = 0.25$ .

## 2 SPLIT-SUM APPROXIMATION

A typical rendering equation needs to compute an integral on the upper hemisphere involving incident light, view direction, normal, and BRDF (Bidirectional Reflectance Distribution Function):

$$c(\omega_o) = \int_{\Omega} L_i(\omega_i) f(\omega_i, \omega_o) (\omega_i \cdot \mathbf{n}) d\omega_i, \quad (6)$$

where  $L_i(\omega_i)$  denotes the light from incident direction  $\omega_i$ ,  $f(\omega_i, \omega_o)$  is the BRDF with respect to the incident direction  $\omega_i$  and outgoing direction  $\omega_o$ , and  $\mathbf{n}$  denotes the surface normal. In practice, the Disney Principled BRDF [McAuley et al. 2013] is the most widely used BRDF, consisting of a diffuse lobe and a specular lobe

$$f(\omega_i, \omega_o) = \underbrace{(1 - \mathbf{m}) \frac{\mathbf{a}}{\pi}}_{\text{diffuse}} + \underbrace{\frac{DFG}{4(\omega_i \cdot \mathbf{n})(\omega_o \cdot \mathbf{n})}}_{\text{specular}}, \quad (7)$$

where  $D$  is the normal distribution function,  $F$  is the Fresnel term,  $G$  is the geometry term,  $\mathbf{a}$  is the albedo, and  $\mathbf{m}$  is the metallicity. However, the integral is expensive to evaluate, and the split-sum

technique [Karis 2013] is an alternative widely used in real-time rendering. The specular term is approximated as

$$c_{\text{specular}} \approx L_{\text{specular}} \cdot ((1 - \mathbf{m}) \times 0.04 + \mathbf{m} \times \mathbf{a}) \times F_1 + F_2, \quad (8)$$

where  $F_1, F_2$  are two scalars from a pre-computed table. The diffuse term is computed as

$$c_{\text{diffuse}} = \frac{\mathbf{a}(1 - \mathbf{m})}{\pi} \cdot L_{\text{diffuse}}. \quad (9)$$

$L_{\text{diffuse}}$  and  $L_{\text{specular}}$  can be directed queried for a pre-filtered environment map or neural light representations. The rendered color  $c(\omega_o)$  is computed as  $c(\omega_o) = c_{\text{diffuse}} + c_{\text{specular}}$ . However, as illustrated in the main paper, with small roughness, the split-sum approximation leads to blurry results.

## 3 LIGHT MODELING

Considering the efficiency of the light query, we use a simple differential environment map and do not model the indirect illumination and occlusion. The environment light is in the cube map format, whose resolution is  $6 \times 512 \times 512$ .

## 4 MORE RESULTS

In this section, we present more results and comparisons.

### 4.1 Glossy Blender Dataset

We present the LPIPS [Zhang et al. 2018] of relighting images on the Glossy Blender dataset in Tab. 1 and Tab. 2. Our method outperforms Gaussian-based methods along with some NeRF-based ones and is competitive with the current SOTA method.

Table 1. Relighting quality with Gaussian-based methods on the Glossy Blender dataset in terms of LPIPS↓.

	GS-IR	RelightGS	GShader	Ours
Angel	0.1901	0.1428	<u>0.1181</u>	<b>0.0858</b>
Bell	0.5203	0.1431	<u>0.1329</u>	<b>0.0795</b>
Cat	0.1591	0.1171	<u>0.1114</u>	<b>0.0596</b>
Horse	0.1606	0.0866	<u>0.0498</u>	<b>0.0356</b>
Luyu	0.1391	0.1094	<u>0.1057</u>	<b>0.0672</b>
Potion	0.2142	0.1614	<u>0.1832</u>	<b>0.0937</b>
Tbell	0.3368	0.1970	<u>0.1877</u>	<b>0.0953</b>
Teapot	0.1716	0.1312	<u>0.1194</u>	<b>0.0982</b>
Mean	0.2365	0.1361	<u>0.1260</u>	<b>0.0769</b>

### 4.2 Shiny Blender dataset

We show the NVS and relighting results on the Shiny Blender dataset [Verbin et al. 2022]. The LPIPS comparison of NVS results is in Tab. 3. We present the relighting result in Fig. 1. Our method provides photo-realistic relighting results, while other Gaussian-based methods fail to render highlights under novel light conditions.

We show decomposed maps in Fig. 2, and our method can provide reasonable BRDF decomposition.

### 4.3 TensorIR synthetic dataset

We present the relighting quality of Gaussian-based methods on the TensorIR synthetic dataset [Jin et al. 2023] in terms of LPIPS in Tab. 4 and the relighting visualization in Fig. 3. The relighting comparison with NeRF-based methods is in terms of PSNR, SSIM in Tab. 5 and LPIPS in Tab. 6. And the relighting visualization of NeRF-based methods is in Fig. 4. We also show the decomposed maps in Fig. 5, and the comparison of normal with Gaussian-based methods in Fig. 6. These results of diffuse objects reveal that though our design focuses on reflective surfaces, it can benefit diffuse objects.

Table 2. Relighting quality with NeRF-based methods on the Glossy Blender dataset in terms of LPIPS↓.

	TensorIR	MII	TensoSDF	NeRO	Ours
Angel	0.2739	0.1404	<u>0.0871</u>	0.1923	<b>0.0858</b>
Bell	0.2806	0.1534	<u>0.0263</u>	<b>0.0189</b>	0.0795
Cat	0.2146	0.1429	0.0675	<b>0.0455</b>	<u>0.0596</u>
Horse	0.2913	0.0713	<b>0.0318</b>	0.0410	<u>0.0356</u>
Luyu	0.2463	0.1393	0.0807	<u>0.0696</u>	<b>0.0672</b>
Potion	0.2954	0.1747	<u>0.0759</u>	<b>0.0623</b>	0.0937
Tbell	0.2786	0.1938	<u>0.0543</u>	<b>0.0407</b>	0.0953
Teapot	0.2030	0.1426	<u>0.0485</u>	<b>0.0193</b>	0.0982
Mean	0.2605	0.1448	<u>0.0590</u>	<b>0.0612</b>	0.0769

Table 3. NVS quality with Gaussian-based methods on Shiny Blender dataset in terms of LPIPS↓.

	GS-IR	RelightGS	GShader	Ours
Ball	0.2966	0.2169	<u>0.1358</u>	<b>0.0842</b>
Car	0.0849	0.0533	<u>0.0477</u>	<b>0.0330</b>
Coffee	0.1125	<b>0.0841</b>	<u>0.0853</u>	0.1035
Helmet	0.1618	0.1014	<u>0.0866</u>	<b>0.0482</b>
Teapot	0.0222	0.0097	<u>0.0108</u>	<b>0.0079</b>
Toaster	0.2479	0.1523	<u>0.1017</u>	<b>0.0859</b>
Mean	0.1543	0.1030	<u>0.0779</u>	<b>0.0605</b>

Table 4. Relighting quality with Gaussian-based methods on the TensorIR synthetic dataset in terms of LPIPS↓.

	GS-IR	RelightGS	GShader	Ours
Armad.	0.0821	<u>0.0593</u>	0.0649	<b>0.0482</b>
Ficus	0.0956	0.0366	<b>0.0437</b>	<u>0.0439</u>
Hotdog	0.1408	<u>0.0880</u>	0.1275	<b>0.0771</b>
Lego	0.1193	<u>0.0902</u>	0.1423	<b>0.0724</b>
Mean	0.1095	<u>0.0685</u>	0.0946	<b>0.0604</b>

Table 5. Relighting quality with NeRF-based methods on the TensorIR synthetic dataset in terms of PSNR↑ and SSIM↑.

	MII	NeRO	TensoSDF	TensorIR	Ours
Armad.	26.85/.9441	23.02/.9335	23.02/.9355	<b>34.51/.9754</b>	31.33/.9593
Ficus	20.65/.9068	<u>27.43/.9404</u>	<b>28.53/.9499</b>	24.32/.9465	26.28/.9542
Hotdog	22.65/.9011	20.45/.9262	20.47/.9241	<b>27.92/.9324</b>	<u>25.21/.9307</u>
Lego	23.20/.8643	17.76/.8577	17.92/.8670	<b>27.61/.9253</b>	<u>25.46/.9083</u>
Mean	23.34/.9041	22.17/.9145	22.48/.9191	<b>28.59/.9449</b>	<u>27.07/.9381</u>

Table 6. Relighting quality with NeRF-based methods on the TensorIR synthetic dataset in terms of LPIPS↓.

	MII	NeRO	TensoSDF	TensorIR	Ours
Armad.	0.0692	0.0644	0.0578	<b>0.0368</b>	<u>0.0483</u>
Ficus	0.0728	0.0677	<u>0.0533</u>	0.0543	<b>0.0439</b>
Hotdog	0.0893	0.0888	<u>0.0906</u>	0.0833	<b>0.0771</b>
Lego	0.1715	0.1228	0.1088	<b>0.0702</b>	<u>0.0723</u>
Mean	0.1007	0.0859	0.0776	<u>0.0612</u>	<b>0.0604</b>

## REFERENCES

- Yingwenqi Jiang, Jiadong Tu, Yuan Liu, Xifeng Gao, Xiaoxiao Long, Wenping Wang, and Yuexin Ma. 2024. GaussianShader: 3D Gaussian Splatting with Shading Functions for Reflective Surfaces. In *CVPR*. IEEE, New York, NY, USA, 5322–5332.
- Haian Jin, Isabella Liu, Peijia Xu, Xiaoshuai Zhang, Songfang Han, Sai Bi, Xiaowei Zhou, Zexiang Xu, and Hao Su. 2023. TensorIR: Tensorial Inverse Rendering. In *CVPR*. IEEE, New York, NY, USA, 165–174.
- Brian Karis. 2013. Real shading in unreal engine 4. *Proc. Physically Based Shading Theory Practice* (2013).
- Bernhard Kerbl, Georgios Kopanas, Thomas Leimkühler, and George Drettakis. 2023. 3D Gaussian Splatting for Real-Time Radiance Field Rendering. *ACM TOG* 42, 4 (2023), 139–1.
- Stephen McAuley, Stephen Hill, Adam Martinez, Ryusuke Villemin, Matt Pettineo, Dimitar Lazarov, David Neubelt, Brian Karis, Christophe Hery, Naty Hoffman, and Hakan Zap Andersson. 2013. Physically based shading in theory and practice. In *ACM SIGGRAPH 2013 Courses (SIGGRAPH '13)*. Association for Computing Machinery, New York, NY, USA, Article 22, 8 pages. <https://doi.org/10.1145/2504435.2504457>
- Dor Verbin, Peter Hedman, Ben Mildenhall, Todd Zickler, Jonathan T. Barron, and Pratul P. Srinivasan. 2022. Ref-NeRF: Structured View-Dependent Appearance for Neural Radiance Fields. In *CVPR*. IEEE, New York, NY, USA, 5491–5500.
- Richard Zhang, Phillip Isola, Alexei A. Efros, Eli Shechtman, and Oliver Wang. 2018. The Unreasonable Effectiveness of Deep Features as a Perceptual Metric. In *CVPR*. IEEE, New York, NY, USA, 10.



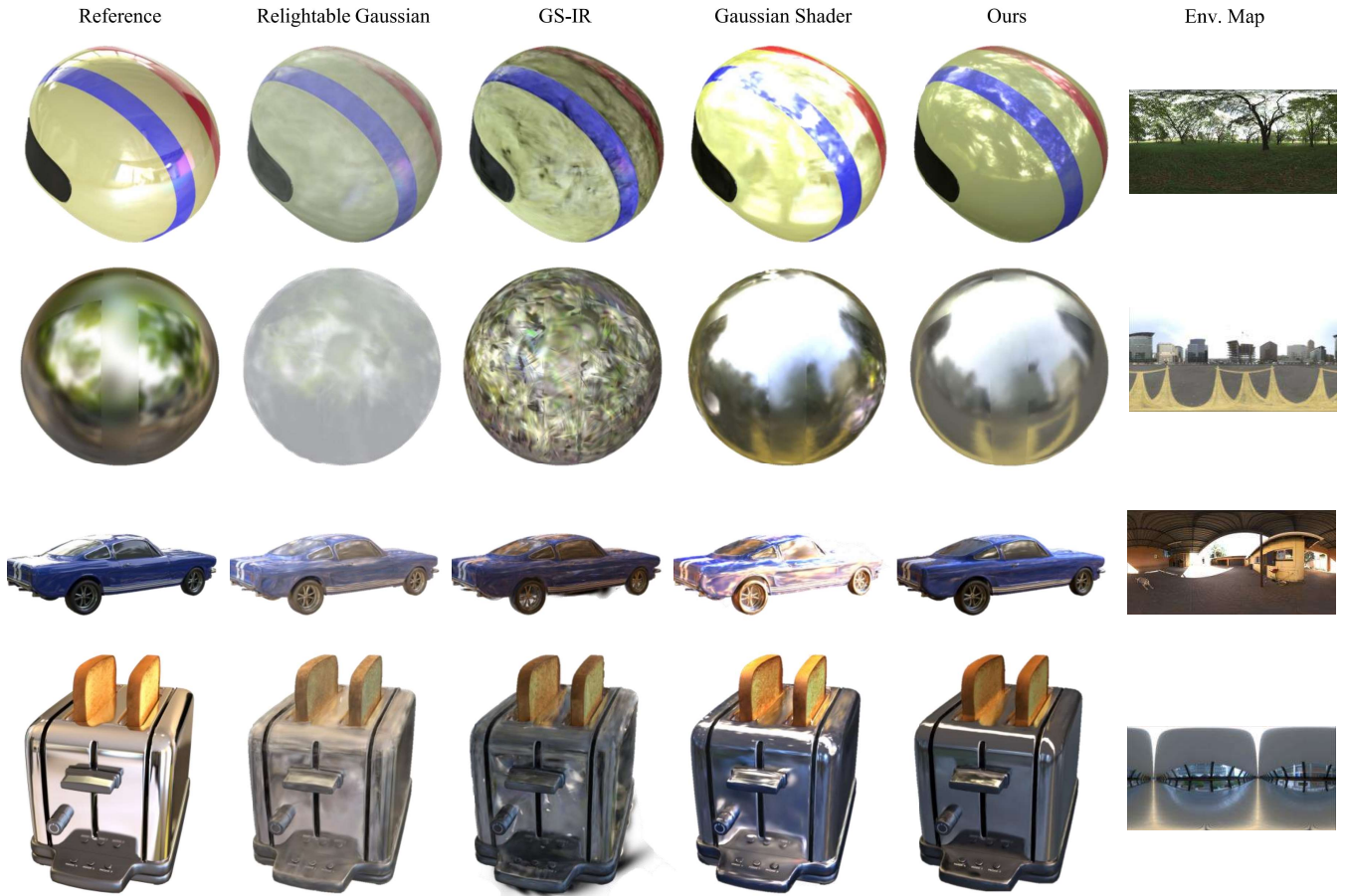


Fig. 1. Relighting results of Gaussian-based methods on the Shiny Blender dataset. Note that no relighting ground truth is available, so we only show the relighting examples. Our method can provide reasonable relighting results under diverse lighting conditions.

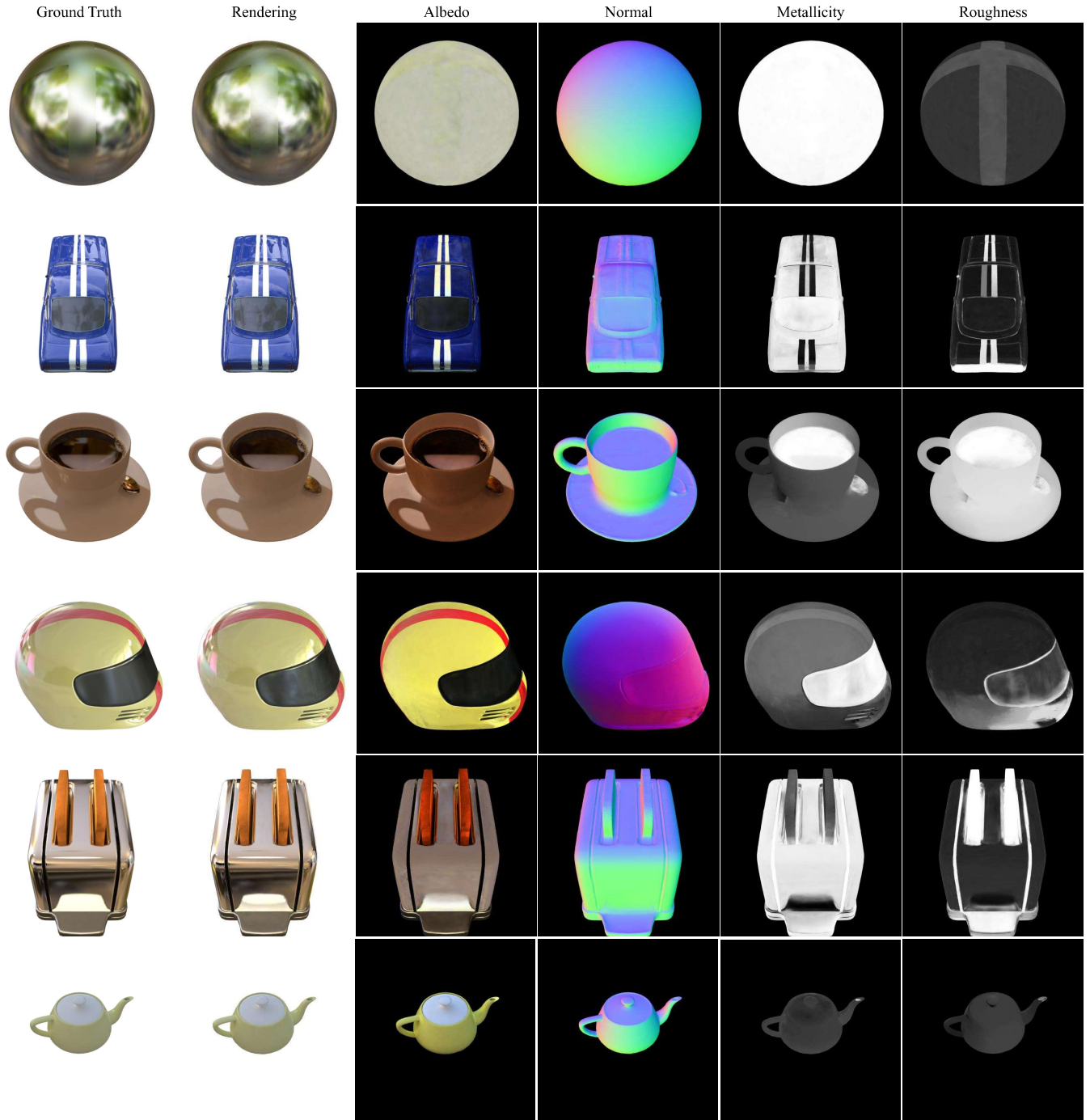


Fig. 2. Normal and BRDF decomposed maps on the Shiny Blender dataset. Our method provides robust normal estimation and reasonable BRDF decomposition.



Fig. 3. Relighting results of Gaussian-based methods on the TensorIR synthetic dataset. Our method can also provide high-quality relighting results for diffuse objects and outperforms the existing Gaussian-based methods.



Fig. 4. Relighting results of NeRF-based methods on the TensoIR synthetic dataset. Our method can also provide high-quality relighting results for diffuse objects and outperforms most NeRF-based methods.



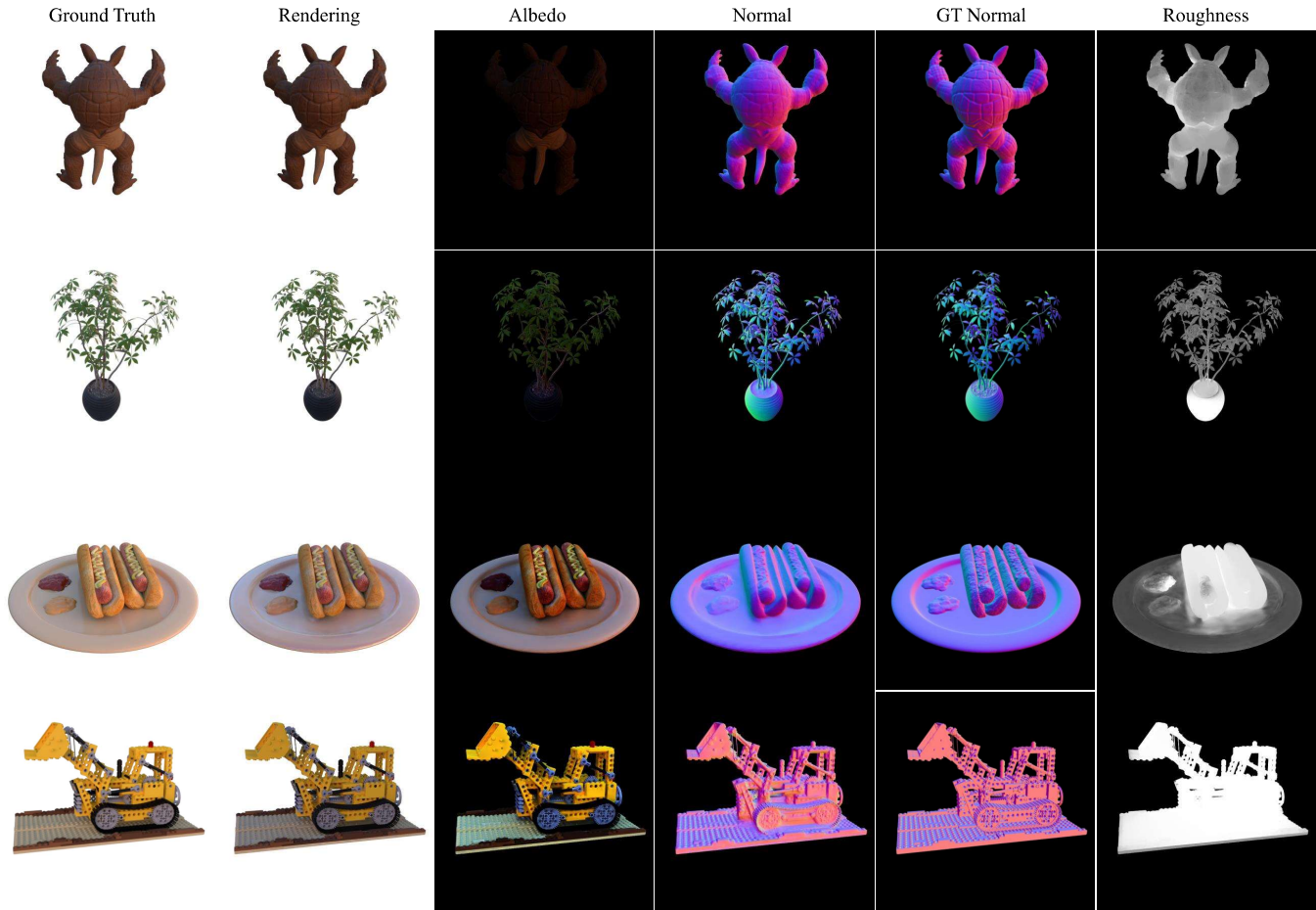


Fig. 5. Normal and BRDF decomposed maps of our method on the TensorIR synthetic dataset. Our method can also provide reasonable BRDF estimation for diffuse objects.

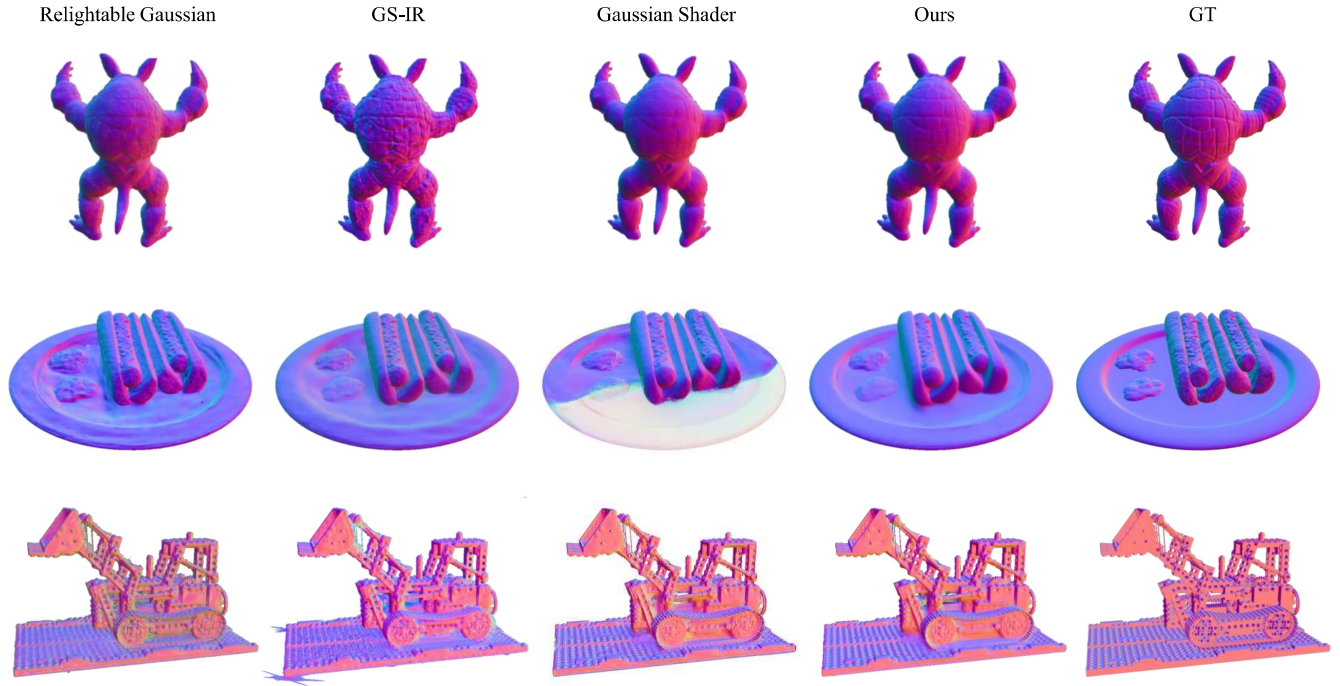


Fig. 6. Normal comparison with Gaussian-based methods on the TensorIR synthetic dataset. Our method can also provide robust normal estimation for diffuse objects.

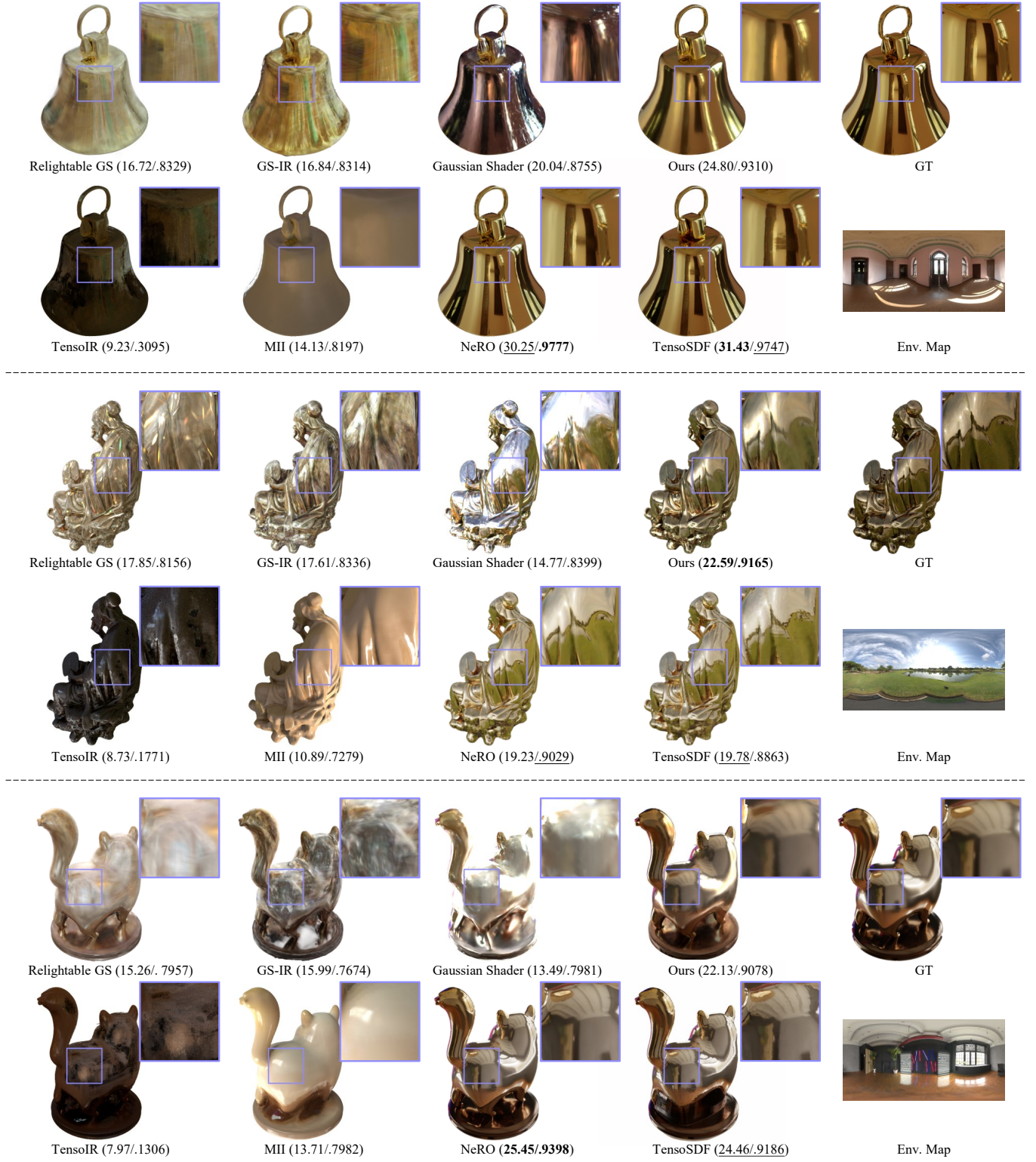


Fig. 10. Relighting results on the Glossy Blender Dataset. Relightable Gaussian, GS-IR, TensoIR, and MII fail to model specular highlights. Gaussian Shader provides specular relighting results with obvious artifacts. Our method, along with NeRo and TensoSDF, provides high-quality results, while our method only uses 25% training time of TensoSDF and enables real-time relighting. We present the metrics per scene (PSNR/SSIM).



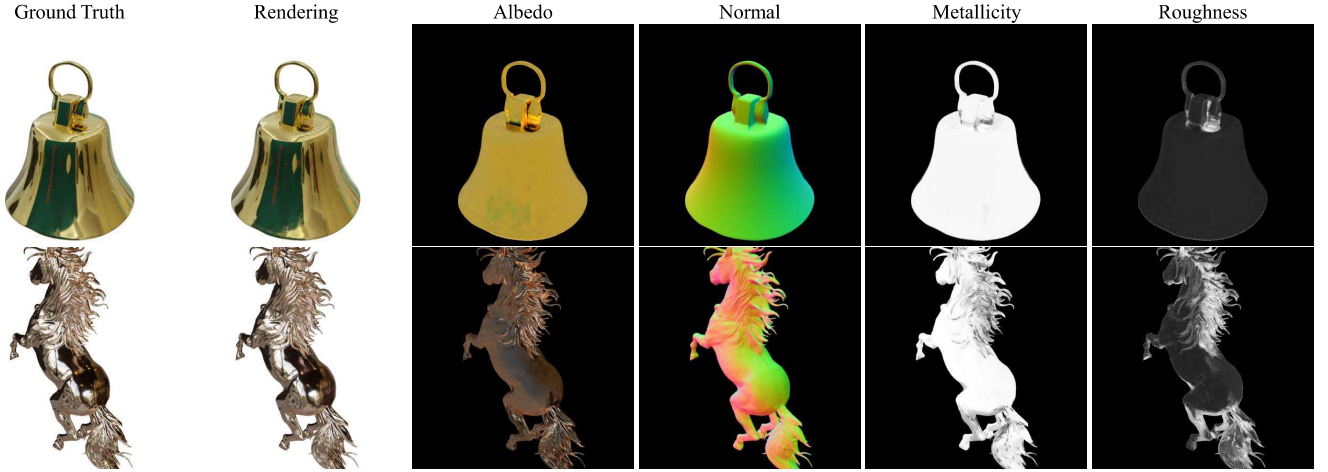


Fig. 11. Decomposed maps of our method on the Glossy Blender Dataset. Our method can provide a reasonable decomposition for reflective surfaces. The normal is smooth but maintains details (see the horse mane in the 2nd row). There is no material ground truth, so we only provide the qualitative visualization.

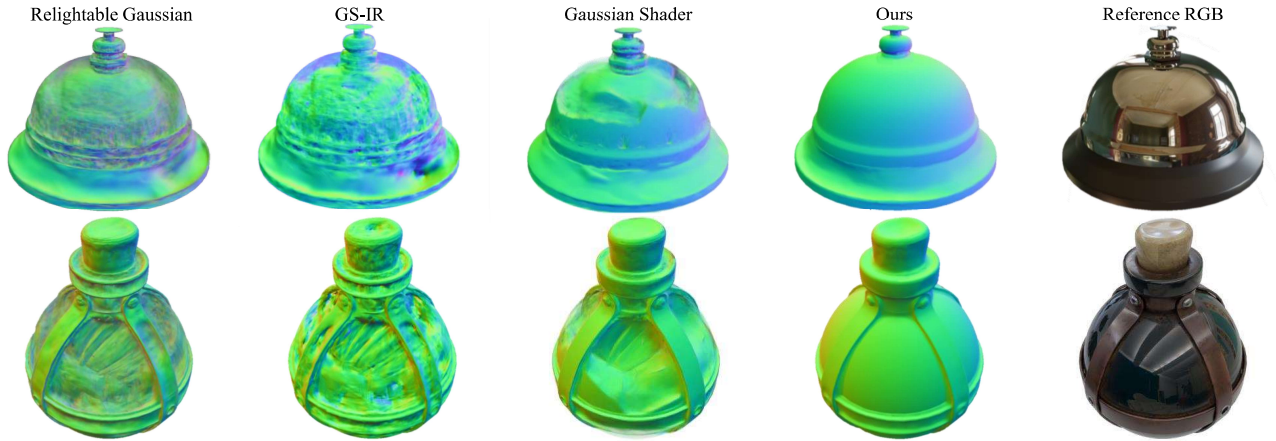


Fig. 12. Normal comparison among Gaussian-based methods on the Glossy Blender Dataset. Our method can reconstruct high-quality normal for relighting, while others overfit under the training scene and provide erroneous normal.



Fig. 13. Relighting results on real data from NeILF++. Relightable Gaussian and GS-IR fail to reconstruct the reflective objects in real scenes. Gaussian Shader cannot relight the specular highlights faithfully, while our method can provide reasonable relighting results.





Fig. 14. NVS results on the Glossy dataset. Our method provides photo-realistic NVS results for reflective objects, while other Gaussian-based methods fail.

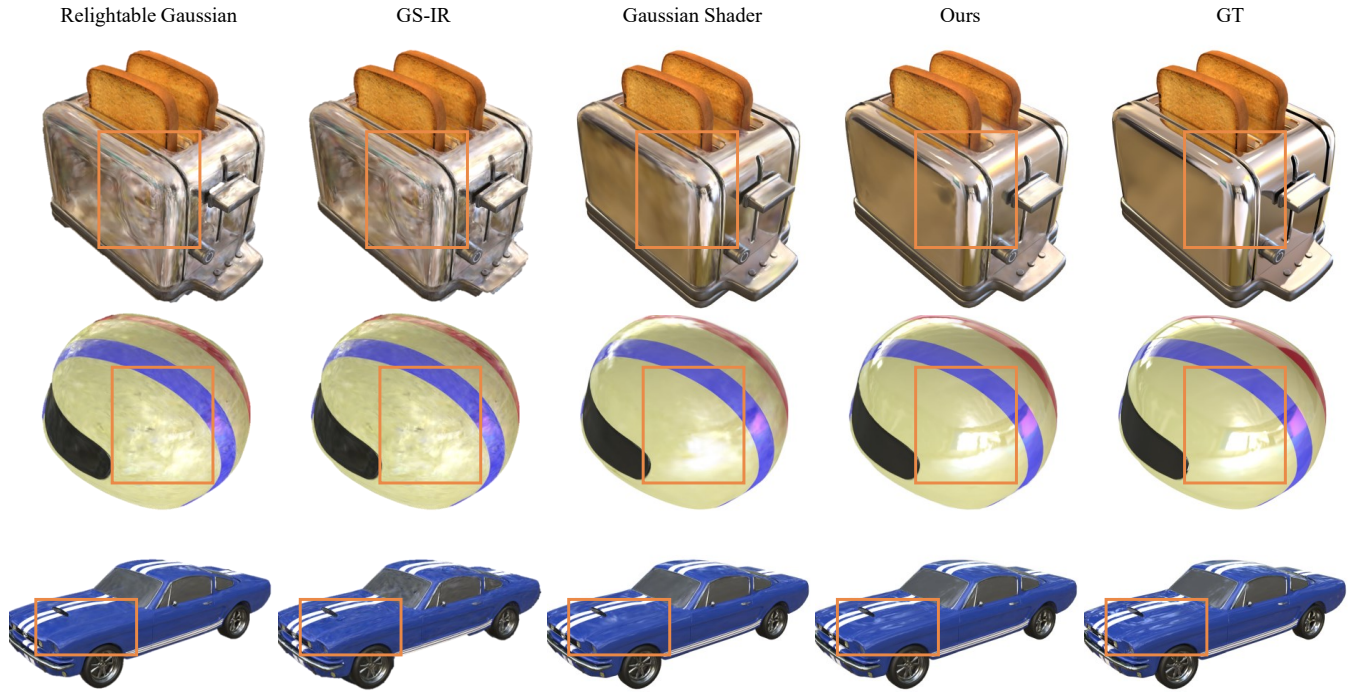


Fig. 15. NVS results of Gaussian-based methods on the Shiny Blender dataset. Our method preserves correct highlights, while others fail to render sharp highlights.

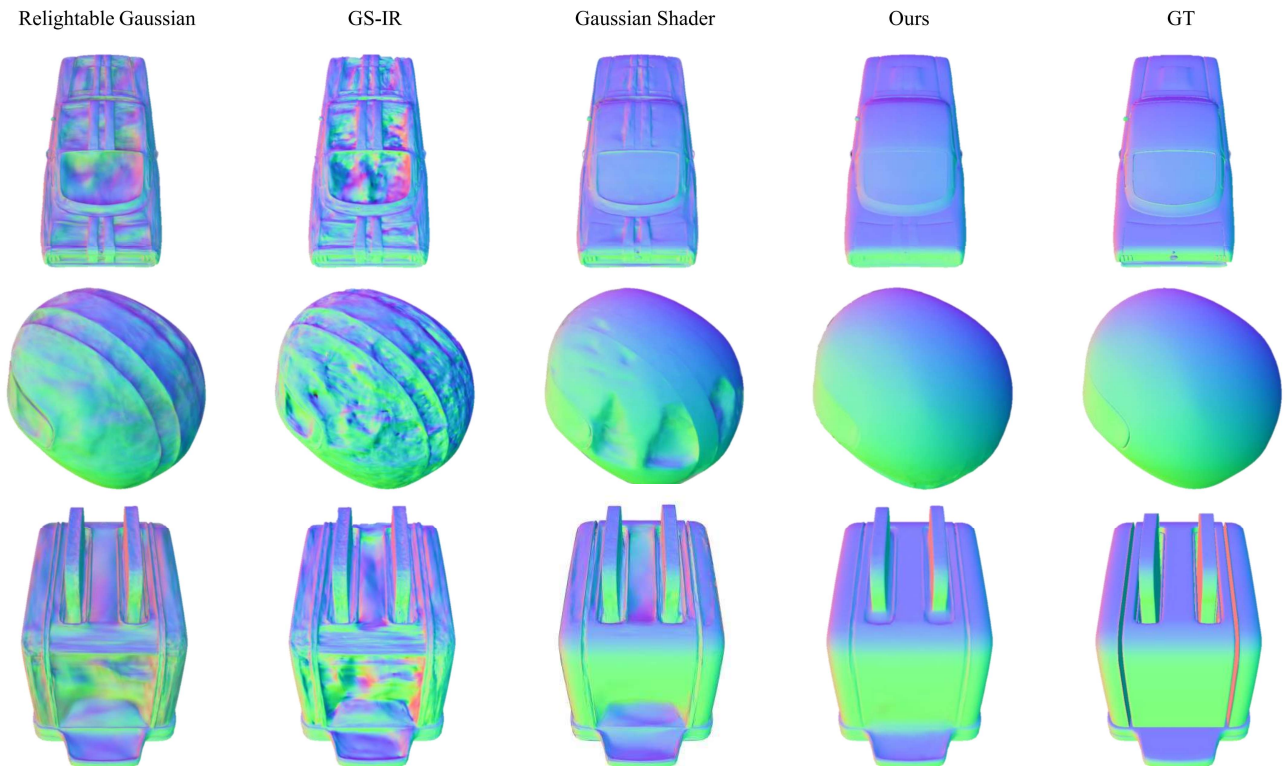


Fig. 16. Normal comparison with Gaussian-based methods on the Shiny Blender dataset. Our method provides robust normal estimation, while other results are noisy or overfitted.